A COMPLETE DYNAMIC MODEL FOR TWIN SCREW EXTRUDERS

S. Choulak * **Y. Le Gorrec** * **F. Couenne** * **C. Jallut** *
P. Cassagnau ** **A. Michel** **

* *LAGEP, UCB Lyon 1, UMR CNRS 5007*
Bat 308 G, 43 Bvd du 11 Nov 1918
69622 Villeurbanne cedex, France
** *LMPB, UMR5627*
ISTIL, 43 Bvd du 11 Nov 1918
69622 Villeurbanne cedex, France

Abstract: A one-dimensional physically motivated dynamic model of a twin-screw extruder for reactive extrusion has been developed. This model can predict extruder behaviour such as pressure, filling ratio, temperature and molar conversion as well profiles as residence time distribution under various operating conditions such as feed rate, screw speed, monomer/initiator ratio and heat flux supplied to the barrel. The model consists of a cascade of perfectly stirred reactors which can be either fully or partially filled with backflow. We consider the mass balance coupled with the momentum balance for the calculation of the pressure profile and the flows between the different reactors. At each reactor is associated the concentration in monomer, the temperature of the matter, the temperatures of the associated piece of screw and barrel. The final model consists of a set of differential algebraic equations. The experimental validation is only made on flow aspects of the model by using experimental RTD's.

Keywords: Reactive extrusion, dynamic model, CSTR, polymerization, residence time distribution, heat transfer

1. INTRODUCTION

A growing interest has emerged in using twin screw extruders as continuous chemical reactors for the polymerisation. Extruders can consequently be used to control the main specific properties of the polymer which are intrinsically linked to the operating pressure and temperature. The primary objective of our research is the control design for polymerization in a twin screw co-rotating extruder. This strategy is applied to the ϵ-caprolactone polymerization. In the case of the regulation of the pressure gradient ΔP at the die, it appears rapidly that the use of simple "grey box" models characterizing an input-output behaviour is not satisfying since the various couplings between all the input variables are not taken into account, see Choulak et al. (2001). This methodology leads to a bunch of simple models, all the bigger as you consider important ranges of variations for manipulated variables (such as feed rate, screw speed, monomer/initiator ratio) since the comportment of the extruder is greatly nonlinear. This approach needs to be able to distinguish between the various models and usually gives rise to synthesize very conservative controls because of the uncertainty of the models. The reader can refer to other publications in the extrusion area

: see Haley and Mulvaney (2000), Tan and Hofer (1995).

Clearly the control of such processes need to have a good understanding of mass flow, rheology, mixing time and thermal behaviour. As far as control is concerned, highly detailed models based on Navier-Stokes equations are not relevant as they are to complicated and do not adress the process modelling but only flowing matter modelling. As far as we know and within the framework of control, he two main references dealing with counter-rotating twin screw extruders are : Ganzeveld et al. (1994) and Graaf et al. (1997) . In these two papers, the description of the material flow along the extruder is intrinsically linked to the model of the C-chamber (which behaves as a CSTR).

In Ganzeveld et al. (1994), the authors consider that the feed in monomer is liquid and then the extruder is formed by two zones : a partially filled zone and a pumping zone (fully filled zone). Thanks to the model of the C-shaped chambers, the pressure and the constant density assumptions, the authors obtain a model issued of mass balance in each chamber represented by differential equations. Moreover the authors couple the energy balance in the barrel to the monomer concentration balance. The main restriction of this model is that there is no accumulation of material in the chambers : the flow profile is fixed. Moreover the length of the fully filled zone is fixed by the die pressure which is an input parameter for the model.

In Graaf et al. (1997), the authors focus on the modelling for predicting the residence time distribution (RTD). The authors consider that the extruder is divided in four zones : the hopper zone (conveying of solid), the partially filled zone (PFZ), a fully filled zone (FFZ) and the die. As previously, the authors obtain a model issued of mass balance in each zone represented by finite differential equations. The main restriction of the model is that the authors fix beforehand the matter occupied volume of each zone; as the result the model cannot predict the flow profile of the extruder and the computation of the gradient pressure is easy.

On the other hand, we find studies concerning food engineering. Four interesting papers emerge : Yacu (1985), Kulshreshta et al. (1991), Kulshreshta and Zaror (1992), and Li (2001). In these four papers are proposed models for twin screw co-rotating extruder taking into account mass and energy balance. The two first papers propose stationary models. The model proposed in Yacu (1985) is the first model predicting axial profile of temperature and pressure in a twin-screw co-rotating extruder. It consists in analytical expressions in the different variables with respect to the spatial coordinate.

It is considered that no heat exchange occurs between the food melt and the screw. Following the zones under consideration (PFZ or CFZ) viscous heat dissipation are negligible or not. In any zone there is heat transfer between the melting and the barrel. The computations of the heat dissipation are based on the work of Martelli (1982). The pressure profile is supposed to be continuous. The computation of the length (related to the pressure profile) of the melt pumping section is made by a trial and error approach. In Kulshreshta et al. (1991), a stationary axial model (from heat and material balances) is presented with the same assumptions. Again the authors consider a simple screw configuration with two zones : the solid conveying zone (PFZ) and the CFZ but their work can be generalized at least theoretically to more than two zones. The continuous treatment of the temperature and pressure profiles leads to a set of differential equations. Again an optimization method is used in order to compute the coordinate of the transition between the two zones in the case of one transition zone. This work was followed by the unsteady version presented in Kulshreshta and Zaror (1992) described by partial differential equations.

In Li (2001) is presented a model for extrusion cooking which is basically the same as in Kulshreshta and Zaror (1992) with two zones (PFZ and CFZ). The difference is in the fact they do not express the mass balance in terms of filling factor but in term of mass flow rate which is continuous. The authors obtain a model described by partial differential equations for temperature and mass flow rate with algebraic constraints for the pressure. The author propose a scheme for integrating these equations.

Finally almost all the authors give models under some restrictive assumptions since many phenomena occur in the extruder :

First, all the authors consider unidirectional analysis. This hypothesis is reasonable since it is not easy to place sensors inside the barrel to measure temperatures, concentrations, flows or information such viscosity. Clearly the model we will build up is also unidirectional. From a process control point of view, the models are often incomplete since energy balance in the screw and the barrel are often not taken into account. It seems to us very important to take these balance into account since in reactive extrusion the problem of controlling the temperature is crucial. We do not found any justification for neglecting their effect.

The second aspect of models is relative to the description of flows along the extruder. The ba-

sic constituent of these models is the C-chamber model which is currently used even for co-rotating extruder. This model is the same as a continuously stirred reactor with direct and pressure-back flows. Thus the authors write the mass and energy balance on this C-chamber. From a geometric point of view, this notion corresponds to a channel. Our vision is more global in the sense that we consider a piece of screw rather than a channel. But the computation of flows follows in the same way. On the other hand, simple screw profiles are used in previous quoted papers. The use of these models to more realistic profiles is not an easy task. Our method, more global, permits to take into account more realistic profiles with an acceptable loss of precision, mixing both geometrical and estimated parameters.

In most of the case, precise rheological and kinetic model are not used. In reactive extrusion the hydrodynamic behavior of the melting is strongly influenced by the rheological properties. In general the melt rheology is supposed to be non-Newtonian. But for the computation of flows, Newtonian behavior is supposed. The computations are easier and remain locally valid.

This paper reports a mathematical unidirectional model for twin-screw extruders. The modelling objective is to predict temperature, concentration and pressure profiles at any time and for a large class of operating conditions. Moreover we present the methodology used to achieve our goal. This is based on a decoupled analysis of the hydrodynamic pattern and the geometry of the extruder. In the next section we present the models used to describe the different phenomena occurring in the reactive extrusion process. In section III, we propose a method to obtain the flow model from the RTD and geometric information. The validation of this model is presented from RTD experiments.

2. THE GEOMETRICAL MODEL

2.1 Description of the extruder geometry

The polymerization is carried out in an intermeshing self-wiping co-rotating extruder (Leistritz LSM $30-34$, centreline distance : $C_1 = 30\ mm$, screw diameter : $D = 34\ mm$, barrel length : $L = 1.2\ m$). The extruder barrel is divided into 10 equal zones. Each zone has individual electrical resistance heaters and a water cooling systems. The screw profile is made up of two blocks of kneading discs, direct screw (right handed elements) and one reverse screw (left handed elements) and the die. The dimension of the tubular die are length $= 10\ mm$, and diameter $= 2\ mm$. The pressure sensors allows to determine the pressure gradient inside the die.

2.2 The flow modelling

The backflow reactor model is chosen as the basic element of the model.

This model has the advantage to represent any element (or a part of an element) of the screw (direct screw elements, reverse screw elements, kneading disk block and the die). The kneading disk block can be considered as a direct screw element or a reverse one according to the staggering angle. The three structures of the basic element are presented in figure 1 ; they correspond to the die, the reverse and direct screw configurations.

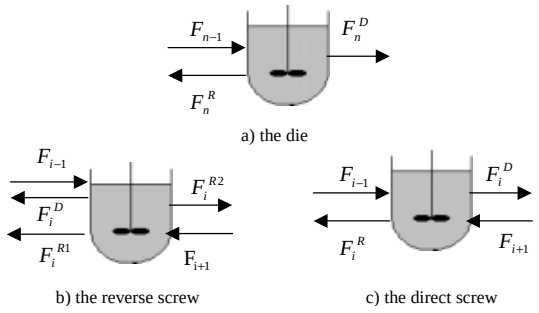

Fig. 1. Structure of the basic elements.

Remark 2.1. The model of the reverse screw element has two pressure depending terms. The F_i^{R1} flow is necessary since without this term the upstream reactors are filled up but not the down stream ones. The flow through the die is considered as being a Poiseuille flow inside a tube.

Let us consider the basic reactor number i as in figure 1.c). This reactor is characterized by its volume and four mass flows. For all these elements, there is no pressure build-up in the partially filled zones and then no reverse flow. In the fully-filled zones, there is a pressure gradient and then a reverse flow occurs. The mass balance for the reactor i leads to :

$$M_i^m \frac{df_i}{dt} = F_{i-1} + F_{i+1} - F_i^D - F_i^R \qquad (1)$$

And for the die :

$$M_n^m \frac{df_n}{dt} = F_{n-1} - F_n^D - F_n^R \qquad (2)$$

The expressions of the direct and reverse flow rates are classical ones obtained from Newtonian hypotheses (see Booy (1980)). The expressions of these flow rates depend on the screw configuration They are given in table 1.

The expressions of the K_i^D's and K_i^R's are functions of the geometry of the screw and of the length of the piece of screw under consideration. The inlet flow rates are equal to the outlet ones when the filling factor of a reactor is equal to one. This leads to the pressure build-up related

Reactor i	F_i^D	F_i^R
Direct pitch	$K_i^D f_i V_i$	if f_i or $f_{i-1} = 1$ $K_i^R(P_i - P_{i-1})$
Reverse pitch	$K_i^D f_i V_i$	if f_i or $f_{i-1} = 1$ $K_i^{R1}(P_{i-1} - P_i)$ if f_i or $f_{i+1} = 1$ $K_i^{R2}(P_i - P_{i+1})$
Die	$K_n^D(P_n - P_a)$	$K_n^R(P_n - P_{n-1})$

Table 1. Expressions of flow rates.(See Booy (1980))

to this reactor and a continuity equation for the mass flow rate. When the filling factor is less than 1, the pressure is supposed to be equal to the atmospheric pressure, say P_a. From a methodological point of view, the computation process is initiated by knowing the profile of filling factor along the extruder. Then the computation of direct flow rate can be done. The profile of pressure is algebraically deduced from the continuity equations (we have to solve a linear system of the type $AP = B$ where A is a matrix, B a vector and P the pressure profile vector. The matrix A is always regular and triangular. When P is obtained, the F_i^R are deduced and equation (1) can be integrated.

2.3 The reaction modelling

The reaction under consideration is the polymerization of the ϵ-caprolactone with tetrapropoxy titanium as initiator. As specified in Gimenez (1999) we consider that the reaction rate is of order 1 with respect to the monomer. The monomer balance is given by equation (3).

$$f_i V_i \mathcal{M} \frac{dC_i}{dt} = (F_{i-1}C_{i-1} + F_{i+1}C_{i+1}) - (F_i^D + F_i^R)C_i - f_i V_i \mathcal{M} K(I_0) e^{-\frac{E}{RT_i^m}} - \mathcal{M} C_i V_i \frac{df_i}{dt} \quad (3)$$

2.4 The thermal modelling

For the sake of simplicity, let us write the energy balance of the melt in the reactor i for direct element (equation (4)). The two first terms of the right member of the equality represent the energy convected by the flowing matter, the third and forth terms, the heat transfer between the melt and the barrel and the heat transfer between the melt and the screw. The two last terms correspond to viscous heat dissipation and the heat flux due to the reaction.

$$\begin{aligned} f_i M_i^m C_p^m \frac{dT_i^m}{dt} &= F_{i-1} C_p^m (T_{i-1}^m - T_i^m) \\ &+ F_{i+1} C_p^m (T_{i+1}^m - T_i^m) + \alpha_b f_i S_b (T_i^b - T_i^m) \\ &+ \alpha_s f_i S_s (T_i^s - T_i^m) + f_i \Psi_i + f_i V_i r(-\Delta H) \end{aligned} \quad (4)$$

In a same way, the energy balance of the associated piece of barrel and of screw can be written.

3. VALIDATION OF THE FLOW MODEL

3.1 The methodology

Let us consider that for a given screw profile, one has discretized the flow by a serial arrangement of N CSTR's with backflows. The model is then able to calculate the time evolutions of the pressure profile, the filling ration profile and the RTD provided that the expressions given in table 1 are sufficiently accurate.

Unfortunately, the number of CSTR's is unknown and expressions given in table 1 are derived from too simple assumptions. Consequently, one has to proceed to some parameters estimation from experimental RTD in order to complete the model. We show that we can predict RTD for new operating conditions after having completed the estimation procedure by using a first set of experimental results. The RTD experiments are performed at steady state.

The screw profile that we use for this study is as follows :

- the matter inlet; a direct element;
a reverse element; a direct element;
a kneading block; a direct element;
the die.

According to the nature and the position of these elements, one can assume that the kneading block as well as the reverse element are completely filled.

The resistive behavior of these elements and of the die implies that a part of the direct elements are also completely filled. These completely filled parts of the direct elements are situated respectively just before the die, the kneading block and the reverse elements.

A serial of five CSTR's with backflows has proved to be sufficient to represent the completely filled zone of the extruder. This zone corresponds approximatively to the dynamic part of the RTD (The RTD without the delay). The tracer balances corresponding to these five CSTR's are then written as follows :

$$\begin{cases} \rho V \frac{dC_1}{dt} &= FC_{in} + F_2^R C_2 - F_1^D C_1 \\ \rho V_2 \frac{dC_2}{dt} &= F_1^D C_1 - (F_2^D + F_2^R)C_2 + F_3^R C_3 \\ \rho V \frac{dC_3}{dt} &= F_2^D C_2 - (F_3^D + F_3^R)C_3 + F_4^R C_4 \\ \rho V_4 \frac{dC_4}{dt} &= F_3^D C_3 - (F_4^D + F_4^R)C_4 + F_5^R C_5 \\ \rho V \frac{dC_5}{dt} &= F_4^D C_4 - FC_5 - F_5^R C_5 \end{cases}$$

where V_2 is the volume of the kneading block, V_5 the volume of the reverse element and V the volume of the three other CSTR's representing the completely filled zone of the direct elements.

Since RTD's are performed in stationary conditions and all the reactors are CF, we have some equalities between flows F to F_5, cf equation (6).

$$F = F_1^D - F_2^R = \cdots = F_4^D - F_5^R \quad (6)$$

To simplify, we suppose to know the direct flow F_{B2} of the reverse screw zone. Finally we have

four unknowns : V, F_2^D, F_3^D, F_4^D. Practically these parameters have been identified.

From the knowledge of the delay in the signal given by the experiment and the feed rate F, the total volume occupied by the matter in the extruder can be computed. From this, the volume occupied by the matter in the PF zones can be deduced.

The partially filled zone of the extruder is also represented by a cascade of CSTR's (it is evident that this partially filled zone is associated to the direct elements). According to relations given in table 1, the reverse flows are equal to 0 in this zone and the tracer balance is as follows for the reactor i :

$$\rho V_{PR} \frac{dC_i}{dt} = FC_{i-1} - FC_i \qquad (7)$$

where V_{PR} is the volume of one CSTR of the partially filled zone (all the CSTR's have the same volume in this zone). The parameter to be estimated is the number of CSTR's necessary to represent the partially filled zone.

One has now to link together the model obtained from the RTD and the geometrical model described by the set of differential algebraic equations. This is done by inserting in the geometrical model at steady state the values of the previously estimated filling ratios. These latter can be computed as soon as a distribution of geometric volume is chosen. It stays a set of equations depending on parameters K_i^D and K_i^R. Fixing the K_i^R's with geometric considerations, and the K_i^D in the CF zone (since these equations are used to compute the pressures), a set of linear equations is obtained. The other K_i^D's are then deduced.

It is clear that this estimation procedure is based on a trial and error method. The discretization based on CSTR's is arbitrarily chosen at the begining and this choice is confirmed by the quality of the results.

3.2 Experimental Validation of the flow modelling

The RTD experiments are carried out with Polypropylene (Polypropylene characteristics are close of the poly-caprolactone characteristics). The estimation procedure is performed by using the experimental RTD obtained for $N = 150$ (rev/mn) and $F = 5\ kg/h$ (see Figure 2). From that point, we can simulate RTD's obtained under other operation conditions (see Figures 3,4 and 5). The identified model is satisfactory as the time delay is well-fitted as well as the shape of the RTD. The poor fitting of figure 4 can be explained by the fact we choose too big volumes for the CF zone. With more suitable choice, the fitting will be better. One can also see on Figure 2 to 5 a comparison between our fitted model and a so called geometrical model based on the following assumptions :

- the number and volume of the CSTR's are the same as the fitted model;
- the direct and reverse flows are calculated by using equations given in table 1.

It can be seen that this geometrical model is not satisfory due to the lack of precision of the expressions given in table 1. The order of magnitude of the direct and reverse flows is good but one has to correct their theoretical predictions from the fitting results.

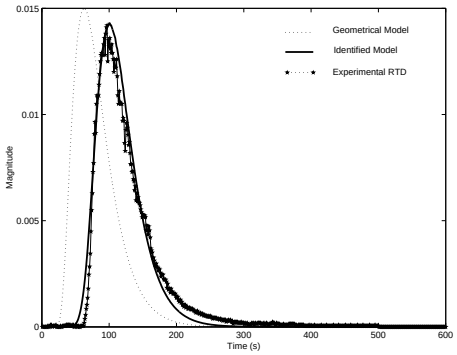

Fig. 2. RTD at screw speed 150 (rev/mn) and flow rate 5 kg/h

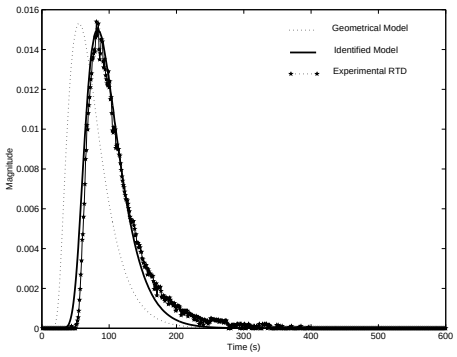

Fig. 3. RTD at screw speed 200 (rev/mn) and flow rate 5 kg/h

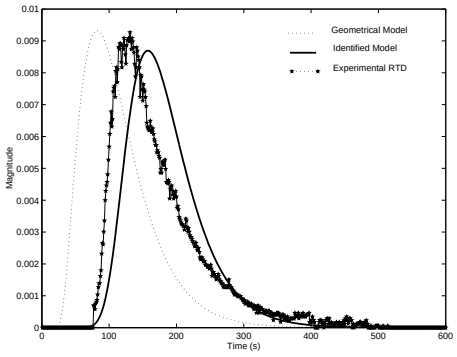

Fig. 4. RTD at screw speed 160 (rev/mn) and flow rate 3 kg/h

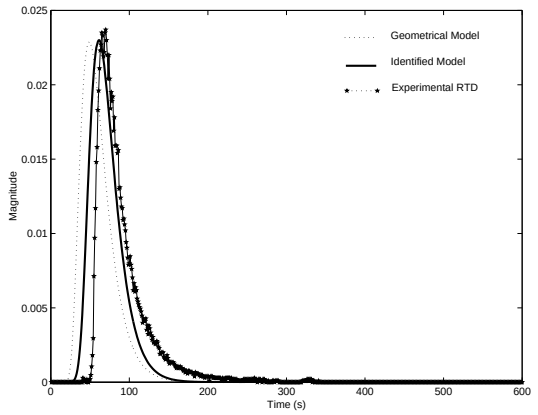

Fig. 5. RTD at screw speed 160 (rev/mn) and flow rate 8 kg/h

4. CONCLUSION

The methodology we have proposed for the extruders dynamic modelling seems to be a right one and give encouraging results. The obtained model can be easily improved by choosing another arrangement of the CSTR's. From the geometric model it can be easily seen that these occupied volumes are different and more important close to the CF zone. Moreover a thermal study of the extruder would give us some additional information on the flow. At this stage, this model can be easily used for control purpose or supervision from a structural point of view even if the model has not been yet entirely validated.

b	: barrel	m	: melt
i	: index of the reactor	s	: screw

Table 2. Subscripts or superscripts.

α_b	: convective heat transfer coefficient of the barrel	$W.m^{-2}.K^{-1}$
α_s	: convective heat transfer coefficient of the screw	$W.m^{-2}.K^{-1}$
Ψ_i	: viscous heat dissipation	W
ΔH	: reaction enthalpy	$J.mol^{-1}$
ρ	: polymer density	$kg.m^3$

Table 3. Greek letters

C_p^m	: specific heat of the melt	$J.kg^{-1}.K^{-1}$
E	: activation energy	$J.mol^{-1}$
f_i	: filling ratio for the reactor i	
F	: feed rate	$kg.s^{-1}$
F_i^D	: direct mass flow rate	$kg.s^{-1}$
F_{i-1}	: mass flow rate coming from the $(i-1)$th reactor	
F_{i+1}	: mass flow rate coming from the $(i+1)$th reactor	
F_i^R	: reverse flow rate produced by reactor i	kgs^{-1}
I_0	: inlet initiator concentration	$mol.m^{-3}$
K	: kinetic constant	s^{-1}
K_i^D	: geometric constant	
K_i^R	: geometric constant	
$\mathcal{M}$	: molar mass of the monomer	$kg.mol^{-1}$
M_i^m	: mass of the melt in the i^{th} reactor	kg
P_a	: atmospheric pressure	Pa
P_i	: i^{th} reactor pressure	Pa
r	: reaction rate	$mol.s^{-1}.m^{-3}$
R	: ideal gas constant	$J.mol^{-1}.K^{-1}$
S_b	: contact surface between the melt and the barrel	m^2
S_s	: contact surface between the melt and the screw	m^2
T_i^m	: temperature of the melt in the reactor i	K
T_i^b	: temperature of the piece of barrel associated to reactor i	K
T_i^s	: temperature of the piece of screw associated to reactor i	K
V_i	: the volume of the reactor i	m^3
N	: rotation speed	$rev.min^{-1}$

Table 4. Notations

REFERENCES

M.L. Booy. Isothermal flow of viscous liquids in corotating twin screw devices. *Polymer Engineering and Science*, 20 (18), 1980.

S. Choulak, F. Couenne, G. Thomas, P. Cassagnau, and A. Michel. Methodology for robust control of pressure for ϵ-caprolactone polymerization in a twin screw extruder. *Chimia*, 55 (3), 2001.

K.J. Ganzeveld, J.E. Capel, D.J. Van Der Wal, and L.P.B.M. Janssen. The modelling of counter-rotating twin screw extruders as reactors for single-component reactions. *Chemical Engineering Science*, 49 (10), 1994.

J. Gimenez. Polymerisation de l' e-caprolactone en extrudeuse : études cinétiques et rhéologiques en vue du contrôle du procédé. *Thèse de doctorat de l'Université Claude Bernard*, 1999.

R.A. De Graaf, M. Rohde, and L.P.B.M Janssen. A novel model predicting the residence-time distribution during reactive extrusion. *Chemical Engineering Science*, 52 (23), 1997.

T.A. Haley and S.J. Mulvaney. On-line system identification and control design of an extrusion cooking process: Part ii. model predictive and inferential control design. *Food Control*, 11 (2), 2000.

M.K. Kulshreshta and C.A. Zaror. An unsteady state model for twin screw extruders. *Trans. IChemE*, 70 (C), 1992.

M.K. Kulshreshta, C.A. Zaror, J. Jukes, and D.L. Pyle. A generalized steady state model for twin screw extruders. *Trans. IChemE*, 69 (C), 1991.

C.H. Li. Modelling extrusion cooking unsteady. *Mathematical and Computer Modelling*, 33, 2001.

F.G. Martelli. Twin screw extrusions: a basic understanding. *Van Nostrand, Reinhold, New York*, 1982.

J. Tan and J.M. Hofer. Self-tuning predictive control of processing temperature for food extrusion. *Journal of Process Control*, 5 (3), 1995.

W.A. Yacu. Modeling a twin screw co-rotating extruder. *Journal of food engineering*, 8, 1985.

A DATA-DRIVEN MODEL FOR VALVE STICTION

M. A. A. S. Choudhury [*] **N. F. Thornhill** [**]
S. L. Shah [*,1]

[*] *Department of Chemical and Materials Engineering*
University of Alberta, Edmonton AB, Canada, T6G 2G6
[**] *Department of Electronic and Electrical Engineering*
University College London, UK, WC1E 7JE

Abstract: The presence of nonlinearities, e.g., stiction, hysteresis and backlash in a control valve limits control loop performance. Stiction is the most common problem in spring-diaphragm type valves, which are widely used in the process industry. Though there have been many attempts to understand the stiction phenomena and model it, there is lack of a proper model which can be understood and related directly to the practical situation as observed in real valves in the process industry. This study focuses on the understanding, from industrial data, of the mechanism that causes stiction and proposes a new data-driven model of stiction, which can be directly related to real valves. It compares simulation results generated using the proposed model with industrial data.

Keywords: stiction, stickband, deadband, hysteresis, backlash, control valve, static friction, viscous friction, nonlinearity, slip jump, control loop performance

1. INTRODUCTION

A typical chemical plant has hundreds or thousands of control loops. Control performance is very important to ensure tight product quality and low cost of the product in such plants. The presence of oscillation in a control loop increases the variability of the process variables thus causing inferior quality products, larger rejection rates, increased energy consumption, and reduced profitability. Bialkowski (1992) reported that about 30% of the loops are oscillatory due to control valve problems. The only moving part in a control loop is the control valve. If the control valve contains static nonlinearities, e.g., stiction, backlash, and deadband, the valve output may be oscillatory which in turn can cause oscillations in the process output. Among the many types of nonlinearities in control valves, stiction is the most common and one of the long-standing problems in the process industry. It hinders the achievement of good performance of a control valve and the control loop. Many studies (Horch, 2000; McMillan, 1995; Horch and Isaksson, 1998; Horch *et al.*, 2000; Aubrun *et al.*, 1995; Wallén, 1997; Taha *et al.*, 1996; Ruel, 2000; Gerry and Ruel, 2001) have been carried out to define and detect on static friction or stiction. However, there is a lack of a unique definition and description of the mechanism of stiction. This work attempts to address this issue and proposes a general definition of stiction. Most of the previous studies are based on some physical model of valve friction. However, parameters of the physical model, e.g., mass of the moving parts of the valve, spring constants and forces, are not explicitly known. These parameters need to be tuned properly to produce the desired response of the valve. The effect of the change in these parameters are also not known. Therefore, working with such a physical model is often time consuming and cumbersome for simulation

[1] author to whom all correspondence should be addressed. E-mail: sirish.shah@ualberta.ca

purposes. Stiction and other related problems are identified in terms of the % of the valve travel or span of the valve input signal. The relationship between the magnitudes of the parameters of a physical model and deadband or backlash or stiction (expressed as a % of the span of the input signal) is not simple. The purpose of this paper is to develop an empirical data-driven model of stiction that is useful for simulation and diagnosis.

2. WHAT IS STICTION?

Different studies or organizations have defined stiction in different ways. Some of the existing definitions of stiction are reproduced below:

- According to the Instrument Society of America (ISA)(ANSI/ISA-S51.1-1979) , *"stiction is the resistance to the start of motion, usually measured as the difference between the driving values required to overcome static friction upscale and downscale"*. The definition was first proposed in 1963 in American National Standard C85.1-1963. Although the people in the process industry do not measure stiction in this way (Ruel, 2000), this definition has not been updated till today.
- According to Entech (1998), *"stiction is a tendency to stick-slip due to high static friction. The phenomenon causes a limited resolution of the resulting control valve motion. ISA terminology has not settled on a suitable term yet. Stick-slip is the tendency of a control valve to stick while at rest, and to suddenly slip after force has been applied"*.
- According to (Horch, 2000), *"The control valve is stuck in a certain position due to high static friction. The (integrating) controller then increases the set point to the valve until the static friction can be overcome. Then the valve breaks off and moves to a new position (slip phase) where it sticks again. The new position is usually on the other side of the desired set point such that the process starts in the opposite direction again"*. This is an extreme case of stiction. On the contrary, once the valve overcomes stiction, it might travel smoothly for some time and then stick again when the velocity of the valve is close to zero.
- In a recent paper (Ruel, 2000) reported *"stiction as a combination of the words stick and friction, created to emphasize the difference between static and dynamic friction. Stiction exists when the static (starting) friction exceeds the dynamic (moving) friction inside the valve. Stiction describes the valve's stem (or shaft) sticking when small changes are attempted"*. This definition of stiction is close to the stiction as measured online by the people in process industries — putting the loop in manual and then increasing the valve input in small increments until there is a noticeable change in the process variable.
- In (Olsson, 1996), stiction is defined as *"short for static friction as opposed to dynamic friction. It describes the friction force at rest. Static friction counteracts external forces below a certain level and thus keeps an object from moving"*.

The above discussion reveals the lack of a formal definition of stiction and the mechanism(s) that cause it. All of the above definitions agree that stiction is the static friction that keeps an object from moving and when the external force overcomes the static friction the object starts moving. But they disagree in the way it is measured and how it can be modelled. Also, there is a lack of clear description of what happens at the moment when the valve just overcomes the static friction. Some modelling approaches described this phenomena using a Stribeck effect model (Olsson, 1996). These issues can be resolved by a careful observation and a proper definition of stiction. From a detailed investigation of real process data it is observed that the phase plot of the valve input-output behavior of a valve "suffering from stiction" can be described as shown in figure 1. It consists of four components: deadband, stickband, slip jump and the moving phase. When the valve comes to a rest or changes the direction (point A in figure 1), the valve sticks. After the controller output overcomes the deadband (AB) plus the stickband (BC) of the valve, the valve jumps to a new position (point D) and continues to move. The deadband and stickband represent the behavior of the valve when it is not moving even though the input to the valve is changing. Slip jump represents the abrupt release of potential energy stored in the actuator chamber as kinetic energy due to high static friction, as the valve starts to move. The magnitude of the slip jump is very crucial in determining the limit cyclic behavior introduced by stiction (McMillan, 1995; Piipponen, 1996). Once the valve moves, it continues to move until it sticks again (point E in figure 1. In this moving phase, dynamic friction which may be much lower than the static friction.

This section has proposed a detailed description of the effects of friction in a control valve and the mechanism and definition of stiction. The definition is exploited in the next and subsequent sections for the evaluation of practical examples and for modelling of valve stiction in a feedback control configuration.

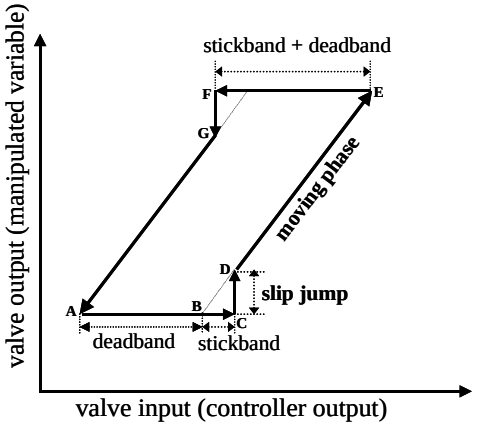

Fig. 1. *Typical input-output characteristic of a sticky valve*

3. PRACTICAL EXAMPLES OF VALVE STICTION

The objective of this section is to observe effects of stiction from the investigation of industrial control loops data. The observations reinforce the need for a rigorous definition of the effects of stiction. This section analyzes two data sets. The first data set is from a power plant and the second is from a petroleum refinery. To preserve the confidentiality of the data sources, all data are scaled and reported as mean-centered with unit variance.

- Loop 1 is a level control loop which controls the level of condensate in the outlet of a turbine by manipulating the flow rate of the liquid condensate. Figure 2 shows the time domain data. The left panel shows time trends for condensate flow rate (pv), the controller output (op) and valve position (mv). The plots in the right panel show the characteristic *pv-op* and *mv-op* plots. The bottom figures clearly show both the deadband plus stickband and the slip jump phenomena. The slip jump is large and visible from the bottom figure especially when the valve is moving in a downscale direction. It is marked as "A" in the figure. It is evident from this figure that the valve output (mv) can never reach the valve input (op). This kind of stiction is termed as the undershoot case of valve stiction in this paper. The *pv-op* plot does not show the jump behavior clearly. The slip jump is very difficult to observe in the $pv - op$ plot because process dynamics (i.e., the transfer between mv and pv) destroys the pattern. This loop shows one of the possible cases of stiction phenomena clearly. The stiction model developed here based on the control signal (op) is able to imitate this kind of behavior.

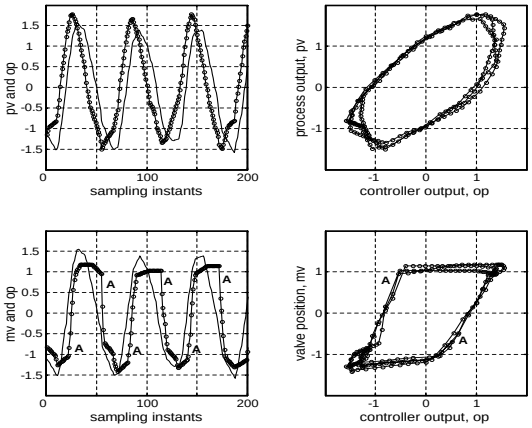

Fig. 2. *Flow control cascaded to level control in an industrial setting, the line with circles is pv and mv, the thin line is op*

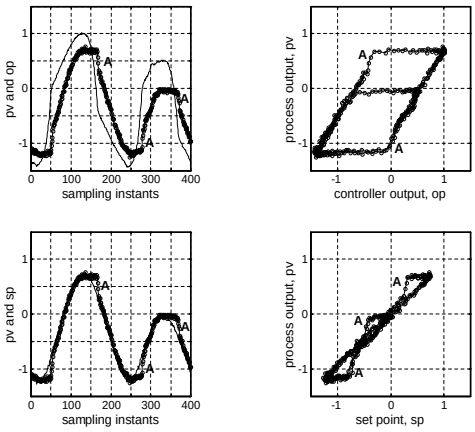

Fig. 3. *Data from a flow loop of a refinery, time trend of pv and op - the line with circles is pv and the thin line is op (top left) and the pv-op plot (top right), time trend of pv and sp - the line with circles is pv and the thin line is sp (bottom left) and the pv-sp plot (bottom right)*

- Loop 2 is a slave flow loop cascaded with a master level control loop. Time trend (Figure 3) shows clearly the undershoot case of stiction. It also shows that the valve has the slip jump phase when it overcomes stiction. Once again this slip jump is not so visible in the characteristic *pv-op* plot of the closed loop data (right panel of the bottom plot in figure 3), but the presence of deadband plus stickband is obvious in the plot. Sometimes it is best to look at the *pv-sp* plot if it is a cascaded loop and the slave loop is operating under proportional control only. The bottom panel of figure 3 shows the time trend and phase plot of sp and pv where the slip jump behavior is clearly visible.

4. DATA DRIVEN MODEL OF VALVE STICTION

A data driven model is useful because the parameters are easy to choose and the effect of these parameter change is simple to understand. The proposed data driven model has parameters that can be directly determined from plant data. The model needs only an input signal and the specification of deadband plus stickband and slip jump parameters.

4.1 *Model Formulation*

According to most industrial personnel, the valve might be sticking only when it is at rest or it is changing its direction. When the valve changes its direction it comes to rest momentarily. Once the valve overcomes stiction, it starts moving and may keep on moving for sometime depending on how much stiction is present in the valve. In this moving phase, it suffers only dynamic friction which is much smaller than the static friction. It continues to move until its velocity is again very close to zero or it changes its direction.

In the process industries, stiction is generally measured as a % of the valve travel or the span of the control signal (Gerry and Ruel, 2001). For example, a 2 % stiction means that when the valve gets stuck it will start moving only after the cumulative change of its control signal is greater than or equal to 2%. If the range of the control signal is 4 to 20 mA then 2% stiction means that a change of the control signal less than 0.32 mA in magnitude will not be able to move the valve. This measure includes the deadband plus stickband. There is no information about the slip jump. To make the model parameters easily understandable by the process people, in our modelling approach the control signal has been translated to the percentage of valve travel with the help of a linear look-up table. The model consists of two parameters -namely deadband plus stickband, 's', and slip jump, 'j'. Figure 4 summarizes the model algorithm.

- First, the controller output (mA) is provided to the look-up table where it is converted to valve travel %.
- If this is less then 0 or more than 100, the valve is saturated.
- If the signal is within 0 to 100% range, it calculates the slope of the controller output signal.
- Then, the change of the direction of the slope of the input signal is taken into consideration. If the sign of the slope changes or remains zero for two consecutive instants, the valve is assumed to be stuck and does not move.

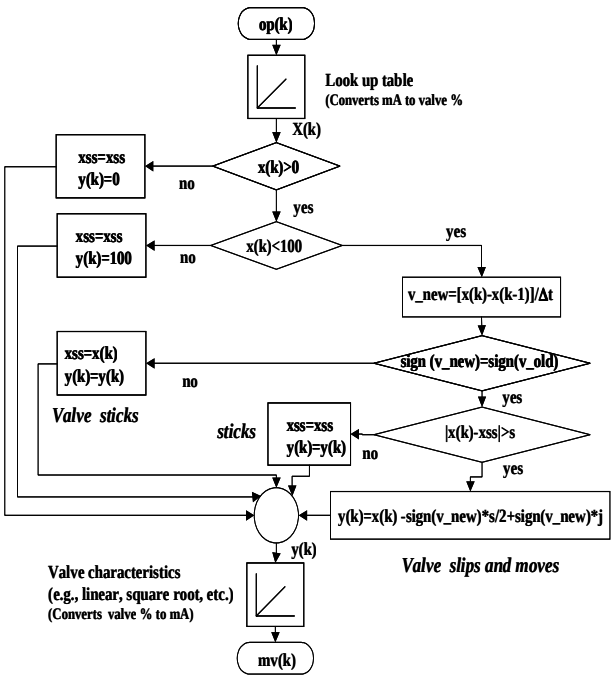

Fig. 4. *Flow chart for algorithm of data-driven stiction model*

- When the cumulative change of the input signal is more than the amount of the stickband (say, "s"), the valve slips and starts moving.
- Finally, the output is again converted back to a mA signal using a look-up table based on the valve characteristics.

The parameter, j signifies the slip jump start of the control valve immediately after it overcomes the deadband plus stickband. It accounts for the offset between the valve input and output signals. Different cases of stiction behavior shown in figure 5 depend on the magnitude of j.

4.2 *Open loop response of the model under a sinusoidal input*

Figure 5 shows the open loop behavior of the new data-driven stiction model in presence of various types of stiction. Plots in the left panel show the time trend of the valve input (thin solid line) and the output (thick solid line). The right panel shows the input-output behavior of the valve on a X-Y plot.

- The first row shows the case of a linear valve without stiction.
- The second row corresponds to the pure deadband without any slip jump, i.e., $j = 0$. Note that for this case, the magnitude of stickband is zero.
- The third row shows the undershoot case of a sticky valve where $j < s/2$. This case is illustrated in the first and second examples of industrial control loops. In this case the

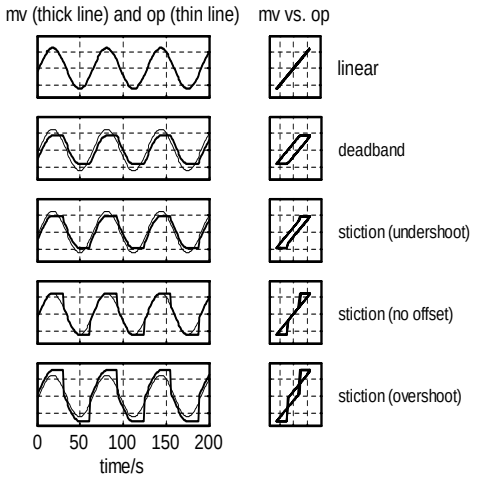

Fig. 5. *Open loop simulation results of the data-driven stiction model*

valve output can never reach the valve input. There is always some offset.

- If $j = s/2$, the fourth row represents pure stick-slip behavior. There is no offset between the input and output. Once the valve overcomes stiction, the valve output tracks the valve input accurately.
- If $j > s/2$, the valve output overshoots the desired set position or the valve input due to excessive stiction. This is termed as overshoot case of stiction.

In reality a composite of these stiction phenomena may be observed. Although this model is not directly based on the dynamics of the valve, the strength of the model is that it is very simple to use for the purpose of simulation and can quantify stiction as a percentage of valve travel or span of input signal. Also, the parameters used in this model are easy to understand, realize and relate to stiction behavior in real life . In future if it becomes possible to find some measure for quantifying stiction from closed loop operating data, it will be easy to translate this measure to the amount of stiction as a % of the span of valve input signal or % valve travel by performing some simulation studies. Though this is an empirical model and not based on physics, it is observed that this model can correctly reproduce the behavior of the physics based stiction model, the results of which are not possible to include here because of space constraints. Also, various type of valve characteristics such as equal percentage, square-root, etc. can easily be incorporated in this model (see figure 4) for further study of flow characteristic type nonlinearities.

4.3 *Closed loop behavior of the data-driven model*

The closed loop behavior of the stiction model has been studied in simulation. Results of two loops are included here, namely a concentration loop and a level loop. The concentration loop has slow dynamics with large dead time. The level loop has only an integrator. The transfer functions, controllers and parameters used in simulation are shown in Table 1. Results for each case are discussed below.

Table 1: Transfer function, controller and parameters for closed loop simulation

Loop type	Transfer function	controller		pure deadband		Stiction (undershoot)		Stiction (no offset)		Stiction (overshoot)	
		K_c	τ_I (s)	s	j	s	j	s	j	s	j
Concentration	$\frac{3e^{-10s}}{10s+1}$	0.2	10	5	0	5	1	5	2.5	5	3.5
Level	$\frac{1}{s}$	0.4	2	3	0	3	0.75	3	1.5	3	2.25

- Concentration loop - The transfer function model for this loop was obtained from (Horch and Isaksson, 1998). This transfer function together with the stiction model was used for closed loop simulation. Steady state results of the simulation are shown in figures 6 and 7. In both figures thin lines are the controller output. The triangular shape of the time trend of controller output is one of the characteristics of stiction (Horch, 2000). In all cases, the presence of stiction causes limit cycling of the process output. In the absence of stiction there are no limit cycles, which is shown in the first row of figure 6. The presence of pure deadband also can not produce any limit cycle. It only adds dead time to the process. This conforms with the findings of (Piipponen, 1996; McMillan, 1995), where they clearly stated that the presence of pure deadband or backlash only adds dead time to the process and the presence of deadband with an integrator produces limit cycle. Figure 6 shows the controller output (op) and valve position (mv). Mapping of mv vs. op clearly shows the stiction phenomena in the valve. But it is not so evident from the mapping of pv vs. op (see figure 7). This mapping only shows some kind of elliptical loops with sharp turn around points. Therefore, if the valve position data is available one should plot valve position (mv) against the controller output (op) instead of pv versus op.
- Level control loop - The closed loop simulation of the stiction model using only an integrator as the process was performed to investigate the behavior of a typical level loop in presence of valve stiction. Results are shown in figure 8. The second row of the figure shows that the deadband can produce oscillations. Therefore with the presence of an integrator in the process dynamics, even

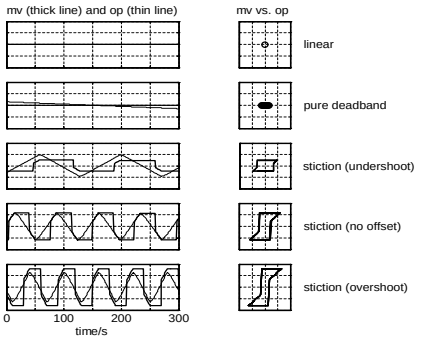

Fig. 6. *Closed loop simulation results of concentration loop, mv and op*

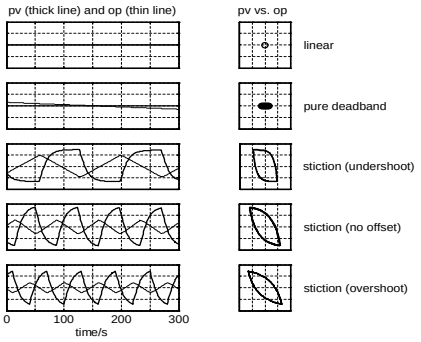

Fig. 7. *Closed loop simulation results of concentration loop, pv and op*

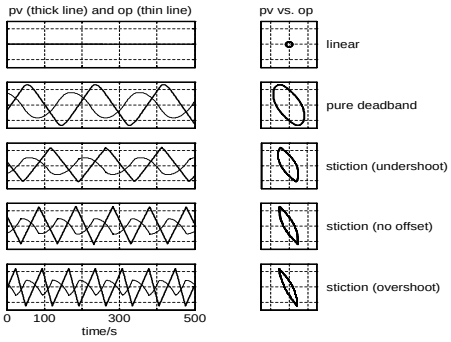

Fig. 8. *Closed loop simulation results of level loop, pv and op*

a pure deadband can produce limit cycles, otherwise the cycle decays to zero. The *pv-op* plots show same kind of elliptical loops with sharp turn around.

5. CONCLUSION

A generalized definition of valve stiction based on the investigation of real plant data has been proposed. Since the physics-based model of stiction is difficult to use because of the requirement of knowledge of mass and forces, a simple yet powerful data-driven empirical stiction model has been developed. Both closed and open loop results have been presented to show the capability of the model. It is recommended that when using a X-Y plot to analyze valve problems one should use the *mv-op* plot instead of the *pv-op* plot.

6. REFERENCES

Aubrun, C., M. Robert and T. Cecchin (1995). Fault detection in control loops. *Control Engineering Practice* **3**, 1441–1446.

Bialkowski, W. L. (1992). Dreams vs. reality: A view from both sides of the gap. In: *Control Systems*. Whistler, BC, Canada. pp. 283–294.

EnTech (1998). *EnTech Control Valve Dynamic Specification (version 3.0)*.

Gerry, John and Michel Ruel (2001). How to measure and combat valve stiction online. http://www.expertune.com/articles/isa2001/StictionMR.htm.

Horch, A., A. J. Isaksson and K. Forsman (2000). Diagnosis and characterization of oscillations in process control loops. In: *Proceedings of the Control Systems 2000*. Victoria, Canada. pp. 161–165.

Horch, A. and A. J. Isaksson (1998). A method for detection of stiction in control valves. In: *Proceedings of the IFAC workshop on On line Fault Detection and Supervision in the Chemical Process Industry*. Session 4B. Lyon, France.

Horch, Alexander (2000). Condition Monitoring of Control Loops. PhD thesis. Royal Institute of Technology. Stockholm, Sweden.

ISA Committee SP51 (1979). Process instrumentation terminology. Technical Report ANSI/ISA-S51.1-1979. Instrument Society of America.

McMillan, G. K. (1995). Improve control valve response. *Chemical Engineering Progress: Measurement and Control* pp. 77–84.

Olsson, H. (1996). Friction in control valves. PhD thesis. Lund Institute of Technology. Sweden.

Piipponen, Juha (1996). Controlling processes with nonideal valves: Tuning of loops and selection of valves. In: *Control Systems*. Chateau, Halifax, Nova Scotia, Canada. pp. 179–186.

Ruel, Michel (2000). Stiction: The hidden menace. *Control Magazine*. http://www.expertune.com /articles/RuelNov2000/stiction.html.

Taha, Othman, Guy A. Dumont and Michael S. Davies (1996). Detection and diagnosis of oscillations in control loops. In: *Proceedings of the* 35^{th} *conference on Decision and Control*. Kobe, Japan.

Wallén, Anders (1997). Valve diagnostics and automatic tuning. In: *Proceedings of the American Control Conference*. Albuquerque, New Mexico. pp. 2930–2934.

A SOFTWARE SENSOR FOR A WASTEWATER TREATMENT PLANT

Teresa Lopez [1], Anna Pulis [2], Michela Mulas[2] and Roberto Baratti [2]

[1] *Instituto Mexicano del Petróleo, Programa de Matemáticas Aplicadas y Computación, A.P. 14-805, 07730 Mexico D.F., Mexico (e-mail: mtlopeza@imp.mx)*
[2] *Dipartimento di Ingegneria Chimica e Materiali, Universita' di Cagliari, Piazza D'Armi, 09123 Cagliari, Italy*

Abstract: In this work, a software sensor is presented in order to monitor the pollutant concentrations in an activated sludge process for industrial and municipal wastewater treatment. The software sensor consists of a model-based state estimator to infer the (unmeasured) biodegradable substrate and ammonia concentrations, based on a reduced process model with approximated model parameters and considering only on-line measurements of dissolved oxygen and nitrate concentrations. The software sensor performance is showed with experimental data from a real process and it is compared versus a complex process model, obtaining good estimated concentrations.

Keywords: Biotechnology, Waste treatment, Detectors, Monitoring, Observability, State estimation.

1. INTRODUCTION

Biological wastewater treatment is an essential operation for the processing of liquid waste, where the main objectives are the degradation of the organic pollutant compounds and the removal of nutrients such as nitrogen that can damage the ecosystem. However during the wastewater treatment, variables such as concentrations are determined by off-line laboratory analysis, making a limitation for on-line monitoring and control purposes. Moreover, a control system design is not straightforward due to (Shimizu, 1996): the lack of reliable sensors, the significant model uncertainty, and the nonlinear time-varying nature of the system.

In a successful manner, concentrations can be on-line estimated using a software sensor (Aubrun et al., 2001; De Asís and Filho, 2000), which consists in using a state estimation technique in combination with a sensor that allows on-line measurements of some process variables, to reconstruct the time evolution of the unmeasured states. Having an important advantage since software sensors can be constructed based on a simple model with uncertain inputs and parameters (Stephanopoulos and San, 1984). Recently, several studies have been reported concerning the software sensor design in wastewater treatment for real time monitoring applications (Aubrun et al., 2001; Bernand et al., 2001; Larose and Jorgensen, 2001; Gomez-Quintero and Queinnec, 2001).

In this work, a software sensor is designed for on-line estimation of the pollutant concentrations in a wastewater treatment. In particular, we are considering a real case: the Tecnocasic plant (located near Cagliari, Italy), which collects industrial and municipal wastewater, and its biological treatment is done by the activated sludge process. The software sensor consists of a model-based state estimator to infer the (unmeasured) biodegradable substrate and ammonia concentrations, based on a reduced process model with approximated parameters and considering on-line measurements of dissolved oxygen and nitrate concentrations. The implementation is done with experimental data from the real process and it is compared versus a complex complete process model.

2. PROCESS MODEL

2.1 Process description

In general, wastewater treatment includes as a first step a mechanical treatment to remove floating and settleable solids, then a biological treatment with activated sludge for removal of nitrogen and other organic pollutants, and after that other operations such as sludge treatment and water chemical treatment.

Here the continuous activated sludge process is considered for the biological wastewater treatment with the main purpose of nitrogen removal. This process (see Fig. 1) includes a reactor divided in two zones: a pre-denitrification step (in an anoxic zone) followed by a nitrification one (in an aerobic zone), and afterward by a settler from which the sludge is partly recirculated to the reactor (return activated sludge, RAS) and partly wasted as excess sludge (waste activated sludge, WAS). The global process is considered isothermal (around 20°C), and both anoxic (with low aeration for mixing purposes) and aerobic (with high aeration for reaction and mixing purposes) zones are controlled by the aeration supply in order to maintain a specific dissolved oxygen set point.

In particular, we are considering a real case: the Tecnocasic plant (located near Cagliari, Italy), which collects industrial and municipal wastewater, and its treatment is done by the activated sludge process as described previously.

2.2 Mathematical modeling

The mathematical modeling was done first by the plant simulation in the GPS-X (a commercial software of Hydromantis), using the two-step-mantis model (Technical reference manual, 2001) which corresponds to the so-called IAWQ Activated Sludge Model No. 1 (Henze et al., 1987) with two modifications: (a) the nitrification is modeled by a two-step process (the conversion of ammonia to nitrite by the nitrosomona bacteria and the conversion of nitrite to nitrate by the nitrobacters), and (b) the hydrolysis of rapidly biodegradable substrate is included. This complex model, that will be referred as GPS-X model, consists of 18 state variables (particle and soluble concentrations) for each anoxic and aerobic reactor, so that the process is modeled with 36 ordinary differential equations, including 15 reaction rates and 30 model parameters. The GPS-X model is included in this work in order to show the advantages of using simple models together with the available measurements, since a great problem for having an exact model is the parameter identification which strongly changes for each waste and biomass type (Maria et al., 2000).

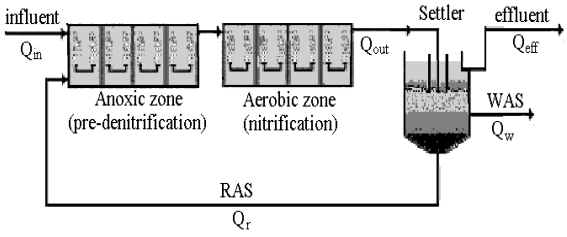

Fig. 1. Diagram of the activated sludge process.

Since we are interested on having estimates of soluble concentrations before the settler, a reduced model proposed by Gomez-Quintero et al. (2000) is considered. Differently from the complete GPS-X model, this model consists of eight state variables:

$$x=[x_1,\ldots,x_8]^T=\left[S^p_{NO_3},S^P_{O_2},S^p_{NH_4},S^p_S,S^n_{NO_3},S^n_{O_2},S^n_{NH_4},S^n_S\right]^T$$

where S_{O2}, S_{NO3}, S_{NH4}, and S_S are the dissolved oxygen, nitrate, ammonia and biodegradable substrate concentrations for each reactor zone (*p* and *n* denote pre-denitrification and nitrification, respectively). The exogenous inputs

$$d=[d_1,\ldots,d_6]^T=\left[S^{in}_{NO_3},S^{in}_{NH_4},S^{in}_S,Q_{in}/V,Q_r/V,Q_w/V\right]^T$$

are the influent concentrations and flow rates. The model needs of only five reaction rates given by

$$r_1^{p/n}=\frac{S_{No3}^{p/n}}{K_{NO3}+S_{No3}^{p/n}},\quad r_2^{p/n}=\frac{K_{O2,H}}{K_{O2,H}+S_{O2}^{p/n}},$$

$$r_3^{p/n}=\frac{S_{NH4}^{p/n}}{K_{NH4}+S_{NH4}^{p/n}},\quad r_4^{p/n}=\frac{S_{O2}^{p/n}}{K_{O2,A}+S_{O2}^{p/n}},$$

$$r_5^{p/n}=\frac{S_{O2}^{p/n}}{K_{O2,H}+S_{O2}^{p/n}}$$

and it has twelve model parameters

$$p=[p_1,\ldots,p_{12}]^T=$$

$$\left[Y_H,i_{XB},K_{O2,H},K_{O2,A},K_{NO3},K_{NH4},\eta_g,\eta_H,\alpha_1,\alpha_2,\alpha_3,\alpha_4\right]^T$$

The reactor model is given as follows:

$$\dot{x}_1=d_1d_4+d_5x_4-(d_4+d_5)x_1-Ax_4r_1^pr_2^p+\alpha_2r_3^pr_4^p$$
$$:=f_1(x_1,x_2,x_3,x_4,x_5,d,p) \quad (1a)$$

$$\dot{x}_2=d_5x_6-(d_4+d_5)x_2+k_{La}^p(S_{OST}-x_2)-Ex_4r_5^p$$
$$-Fr_3^pr_4^p:=f_2(x_2,x_3,x_4,x_6,d,p) \quad (1b)$$

$$\dot{x}_3=d_2d_4+d_5x_7-(d_4+d_5)x_3-Bx_4(r_5^p+r_1^pr_2^p)$$
$$-\alpha_2r_3^pr_4^p+\alpha_3:=f_3(x_1,x_2,x_3,x_4,x_7,d,p) \quad (1c)$$

$$\dot{x}_4=d_3d_4+d_5x_8-(d_4+d_5)x_4+(\alpha_4-Dx_4)r_5^p+$$
$$(C-Dx_4)r_1^pr_2^p:=f_4(x_1,x_2,x_4,x_8,d,p) \quad (1d)$$

$$\dot{x}_5=(d_4+d_5)(x_1-x_5)-Ax_8r_1^nr_2^n+\alpha_2r_3^nr_4^n$$
$$:=f_5(x_1,x_5,x_6,x_7,x_8,d,p) \quad (1e)$$

$$\dot{x}_6 = (d_4 + d_5)(x_2 - x_6) + k_{La}^n (S_{OST} - x_6) - Ex_8 r_5^n - Fr_3^n r_4^n := f_6(x_2, x_6, x_7, x_8, d, p) \quad (1f)$$

$$\dot{x}_7 = (d_4 + d_5)(x_3 - x_7) - Bx_8 (r_5^n + r_1^n r_2^n) - \alpha_2 r_3^n r_4^n + \alpha_3 := f_7(x_3, x_5, x_6, x_7, x_8, d, p) \quad (1g)$$

$$\dot{x}_8 = (d_4 + d_5)(x_4 - x_8) + (\alpha_4 - Dx_8) r_5^n + (C - Dx_8) r_1^n r_2^n := f_8(x_4, x_5, x_6, x_8, d, p) \quad (1h)$$

where

$$A = \alpha_1 (1 - Y_H)/2.86 Y_H \;,\quad B = \alpha_1 i_{XB} \;,\quad C = \alpha_4 \eta_h$$
$$D = \alpha_1 / Y_H \;,\quad E = \alpha_1 (1 - Y_H)/Y_H \;,\quad F = 4.57\alpha_2$$

2.3 Test motion

As it was mentioned before, the experimental data correspond to the Tecnocasic plant (Cagliari, Italy) for industrial and municipal wastewater treatment. The experimental motion is shown in Fig. 2 (where the data were taken one per day), with an operation condition around the mean value $\bar{d} \approx$ [0.0 gN/m^3, 16.25 g N/m^3, 118.3 g COD/m^3, 3.10 d^{-1}, 3.90 d^{-1}, 0.28 d^{-1}]^T with some disturbances. For the dissolved oxygen control, a PI-controller was used to calculate the airflow supply to each reactor (equivalent to calculate the necessary oxygen mass transfer coefficient, k_{La}). And the identified model parameters (according Gomez-Quintero et al., 2000) are given in Table 1.

In Fig. 2 the test motion for the two considered models are shown in comparison with the experimental one. As we can see, the GPS-X model gives a very good approximation, while the reduced model gives the motion tendency but with significant offsets due to the errors in the model assumptions and parameter identification. With these results, it can be stated one of the tasks that the software sensor should do: using the reduced model, the software sensor should give a good inference of the modeling errors in order to reach the actual (experimental) concentration motions.

Table 1. Reduced model parameters

Parameter (p)	Value
Y_H	0.7
i_{XB}	0.086 g N (g COD)$^{-1}$
$K_{O2,H}$	0.2 g O_2 m^{-3}
$K_{O2,A}$	0.23 g O_2 m^{-3}
K_{NO3}	0.1 g N m^{-3}
K_{NH4}	0.8 g NH_3-N m^{-3}
η_g	0.5
η_H	0.4
α_1	163.9 d^{-1}
α_2	224.63 g m^{-3}d^{-1}
α_3	92.12 g m^{-3}d^{-1}
α_4	739.74 g m^{-3}d^{-1}

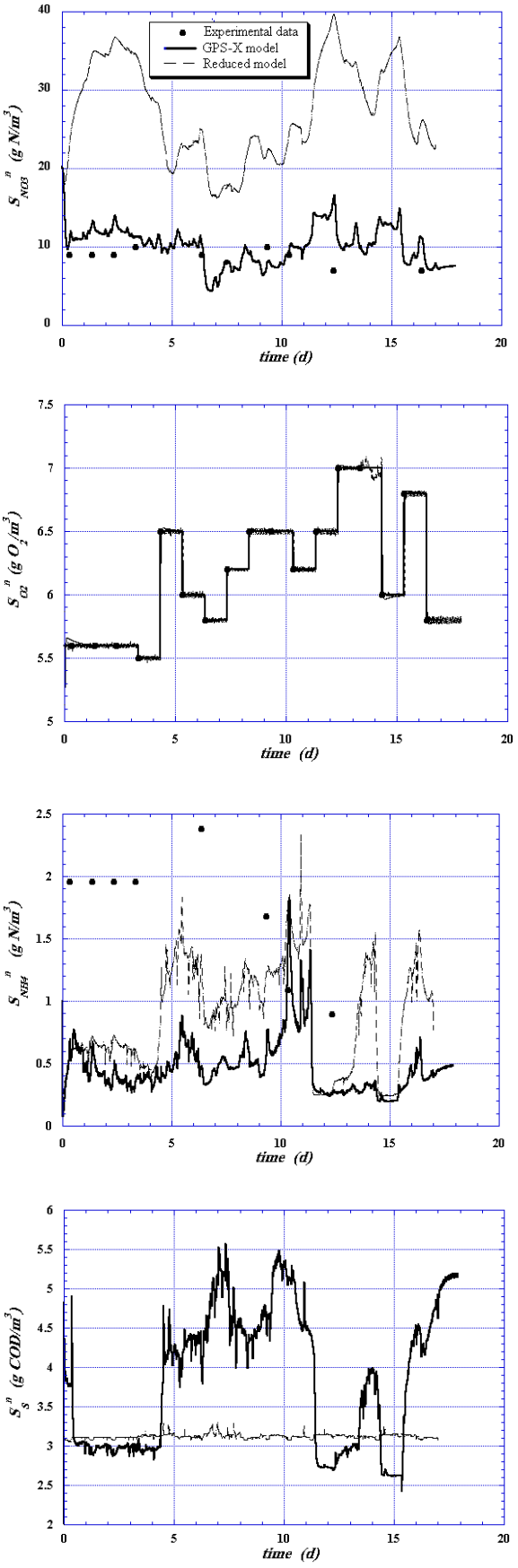

Fig. 2. Performance of the GPS-X (———) and reduced (– – – –) models, in comparison with the experimental data (•).

2.4 On-line monitoring problem

In our experimental study, the on-line monitoring problem consists on designing a software sensor for estimating mainly the ammonia and biodegradable substrate concentrations in the reactor exit (before the settler), from available measurements of dissolved oxygen in both reactor zones and the ammonia concentration in the (aerobic) nitrification zone. Meaning that the measured output is given by

$$y = \left[y_1, y_2, y_3\right]^T = \left[S_{O2}^p, S_{NO3}^n, S_{O2}^n\right]^T \tag{2}$$

The software sensor will be based on the reduced model [Eqs. (1)] and these three measurements [Eq. (2)], and it should be robust to have tolerance to the modeling error and to the uncertain inputs and measured outputs.

3. SOFTWARE SENSOR DESIGN

For this purpose, the design is based on the geometric nonlinear estimation methodology developed in Alvarez and Lopez (1999) and Lopez (2000), which has a systematic construction, with a robust convergence criterion connected to the convergence rate, and with a simple tuning procedure.

Next the observability analysis, the estimator construction and tuning are presented for our specific case study.

3.1 Observability analysis

According to Alvarez and Lopez (1999), the motion x(t) of the reactor [Eqs. (1) and (2)] is *RE (robustly exponentially) - detectable* (i.e. partial observable) with the observability indices

$$(\kappa_1, \kappa_2, \kappa_3)^T = (2, 2, 2)^T \tag{4}$$

and with the state partition (x_I and x_{II} are the observable and unobservable states, respectively)

$$x_I = \left[x_2, x_3, x_5, x_6, x_7, x_8\right]^T \tag{5a}$$

$$x_{II} = \left[x_1, x_4\right]^T \tag{5b}$$

if the two following conditions are met along the reactor motion x(t):

(i) The map $\phi(x, d, p)$ is invertible for x_I, and
(ii) The motions of the unobservable dynamics $x_{II}(t)$ are stable.

Where the map ϕ is given by the measured outputs and some of their time-derivatives:

$$\phi\left(x,d,p\right) = \left[y_1, \dot{y}_1, y_2, \dot{y}_2, y_3, \dot{y}_3\right]^T$$

$$= \left[x_2, f_2\left(x,d,p\right), x_5, f_5\left(x,d,p\right), x_6, f_6\left(x,d,p\right)\right]^T \tag{6}$$

To verify that the plant is detectable for all time, next the two conditions are verified.

Assessment of the invertibility condition. Here it is important to mention that the observability matrix Q corresponds to

$$Q = \frac{\partial \phi}{\partial x_I} \tag{7}$$

Such that the invertibility condition [condition (i)] is equivalent to verify that $Rank[Q] = \kappa_1 + \kappa_2 + \kappa_3 = 6$, or else, $det[Q] \neq 0$ for all time. In fact this condition was evaluated numerically as can be seen in Fig. 3, showing that $det[Q] < 0$ for all time.

Assessment of the stability condition. The stability condition [condition (ii)] is equivalent to verify that the dynamics of

$$\dot{x}_1 = f_1\left(x_1, \bar{x}_2, \bar{x}_3, x_4, \bar{x}_5, \bar{d}\right) \tag{8a}$$

$$\dot{x}_4 = f_4\left(x_1, \bar{x}_2, x_4, \bar{x}_8, \bar{d}\right) \tag{8b}$$

are stable, considering $\bar{x}_2$, $\bar{x}_3$, $\bar{x}_5$, $\bar{x}_8$ and $\bar{d}$ as nominal known motions. These equations are stable if the eigenvalues of its linear system have strictly negative real part. This is verified also numerically along the reactor motion and is shown in Fig. 4, concluding that the unobservable dynamics are stable.

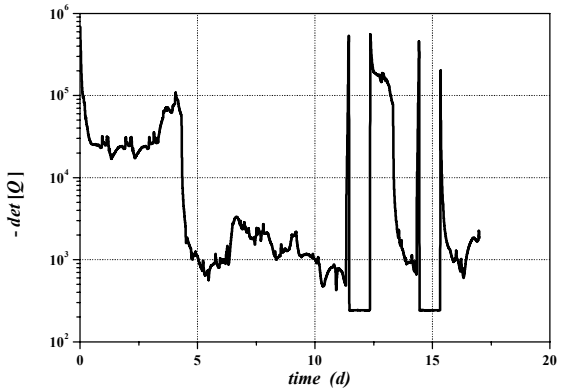

Fig. 3. Determinant of the observability matrix.

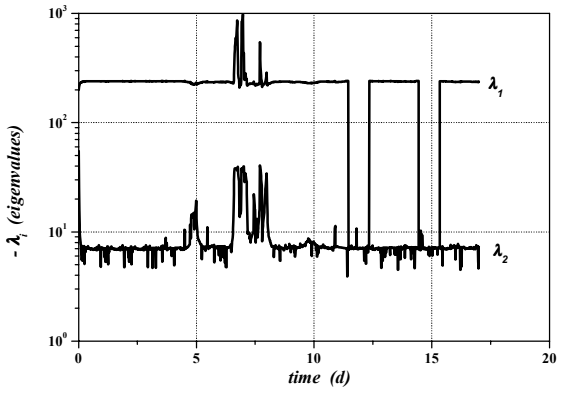

Fig. 4. Eigenvalues of the unobservable dynamics.

As the two conditions are met, therefore the reactor motion is RE-detectable, and a state estimator can be implemented.

3.2 Construction

Considering the previous state partition [Eqs. (5)], the plant [Eqs. (1) and (2)] can be rewritten as

$$\dot{x}_I = f_I\left(x_I, x_{II}, d, p\right) \tag{9a}$$

$$\dot{x}_{II} = f_{II}\left(x_I, x_{II}, d, p\right) \tag{9b}$$

$$y = h\left(x_I\right) \tag{9c}$$

The construction of the geometric estimator (Luenberguer-like high-gain) follows from a straightforward consequence of the detectability property, according to the following expression (see Theorem 1 in Alvarez and Lopez, 1999). So that the estimator for our case is given by

$$\dot{\hat{x}}_I = f_I\left(\hat{x}_I, \hat{x}_{II}, d, p\right) + Q^{-1}K_o\left[y - h\left(\hat{x}_I\right)\right] \tag{10a}$$

$$\dot{\hat{x}}_{II} = f_{II}\left(\hat{x}_I, \hat{x}_{II}, d, p\right) \tag{10b}$$

$$\hat{y} = h\left(\hat{x}_I\right) \tag{10c}$$

Here Q^{-1} is the inverse of the observability matrix [Eq. (7)], and K_o is the gain matrix which should be chosen such that the estimation error dynamics are stable (this will be discussed in next subsection). It can be seen that the observable part [Eq. (10a)] of the estimator has two terms: (i) a predictor term given by the model, and (ii) a corrector term driven by the error in the measurements. While the unobservable part [Eq. (10b)] only has a predictor term given by the model.

3.3 Tuning

Some strategies for the estimator tuning are also given in Alvarez and Lopez (1999) and Lopez (2000). According to this, the gains can be calculated as follows

$$K_o = \begin{bmatrix} k_{11} & 0 & 0 \\ k_{12} & 0 & 0 \\ 0 & k_{21} & 0 \\ 0 & k_{22} & 0 \\ 0 & 0 & k_{31} \\ 0 & 0 & k_{32} \end{bmatrix}, \qquad \begin{aligned} k_{i1} &= 2\zeta\omega_i \\ k_{i2} &= \left(\omega_i\right)^2 \end{aligned} \tag{11}$$

Where ζ is the damping factor, which can be set according the literature (Stephanopoulos, 1984) as $\zeta = 0.71$ in order to have a response with moderate oscillations. While ω_i is the characteristic frequency, which can be selected such that the estimator response is faster than the reactor response. For this purpose, first we calculated the residence time as $\theta = 0.1428$ d, then to obtain an estimator response faster, we selected the estimator characteristic time as $\omega_i > 10 / \theta$. Meaning that a good initial test can be $\omega_i = 70\ d^{-1}$. In fact after some trials, the final tuning values were set as $\omega_1 = \omega_2 = \omega_3 = 150\ d^{-1}$ ($\approx$ 20 times faster than the natural dynamics).

5. IMPLEMENTATION RESULTS

Here it is worth of mention that the experimental data (shown in Fig. 2) are off-line laboratory analysis taken one per day, however with purpose of implementation of the software sensor [Eqs. (10)], the outputs [Eq. (2)] are incorporated as on-line measurements. So that when the software sensor is implemented there is exact converge for the measured states ($S^p_{O2}, S^n_{NO3}, S^n_{O2}$) as was expected, while for the other states good estimates are obtained. In Fig. 5, the inference of the two main (ammonia S^n_{NH4} and biodegradable substrate S^n_S) concentrations of interest in the reactor exit is shown. In this figure, we can see that the estimated ammonia concentration reaches closely the experimental data, in fact better than the GPS-X model estimation (shown in Fig. 2). With this result, we can say that the biodegradable substrate estimation should be reliable, in spite of no having experimental data for comparison.

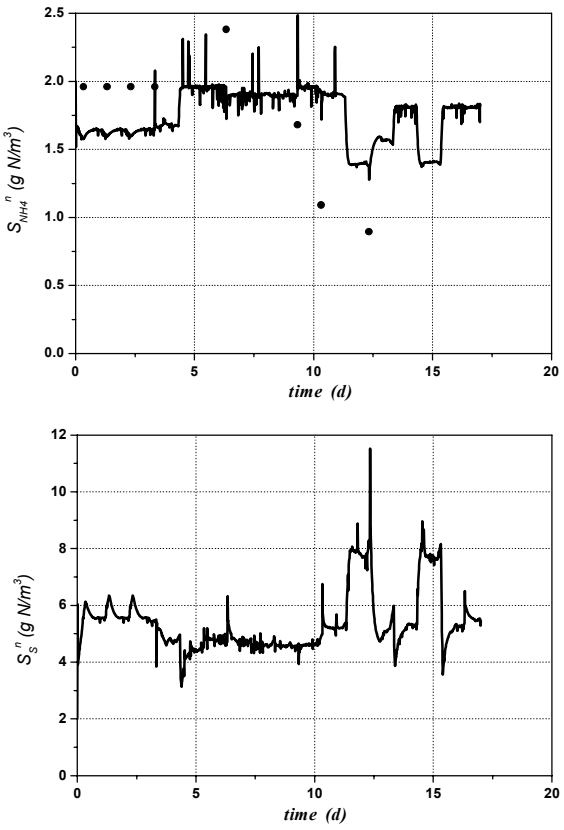

Fig. 5. Software sensor (———) in comparison with the off-line experimental data (•).

6. CONCLUSIONS

In this study, the on-line estimation of unmeasurable concentrations of ammonia and biodegrable substrate in a wastewater treatment has been investigated, using a software sensor based upon a reduced model and considering only on-line measurements of dissolved oxygen and nitrate concentrations. The positive results, validated with experimental data, displays that the estimated concentrations are reliable in spite of the presence of input disturbances and of using a simple reduced model with uncertain parameters. Showing that not always the use of complex models is the best way to obtain a good process representation for monitoring and control purposes.

The solution of using a software sensor gives promising guidelines to tackle in the future the problem of real time control of wastewater treatment plants.

Acknowledgments. The work was supported by a contribution from MIUR (2002095147). The authors are very grateful to the Instituto Mexicano del Petroléo (MEXICO) and to the Regione Sardegna.

NOMENCLATURE

d	exogenous input
f	model map
i_{XB}	Mass N/ mass COD in biomass
K_o	observability matrix gain
k_{La}	oxygen mass transfer coefficient (d^{-1})
$K_{O2,H}$	Aerobic oxygen half-saturation coefficient
$K_{O2,A}$	Aerobic/anoxic oxygen half-sat. coefficient
K_{NO3}	Nitrate half-saturation coefficient
K_{NH4}	Ammonia half-saturation coefficient
p	model parameter
Q	observability matrix
Q_n	flow rate, m^3/d (n = *in, out, r, w*)
r_i	i-th reaction rate ($1 \le i \le 5$)
S_{NO3}	nitrate concentration (g N/m^3)
S_{O2}	dissolved oxygen concentration (g O_2/m^3)
S_{NH4}	ammonia concentration (g N/m^3)
S_S	biodegradable substrate conc. (g COD/m^3)
S_{OST}	dissolved oxygen saturation conc. (g O_2/m^3)
V	reactor volume (m^3)
x	process state
y	measured output
Y_H	Heterotrophic yield

Greek symbols

α_i	i-th reduced model parameter ($1 \le i \le 4$)
η_g	Correction factor for anoxic growth
η_H	Correction factor for anoxic hydrolysis
ϕ	observable map
κ_i	observability index ($1 \le i \le 3$)
ζ	damping factor
ω_i	characteristic frequency ($1 \le i \le 3$)

Subscripts

in	influent
r	RAS
w	WAS
out	reactor exit
eff	(clean) effluent
I	observable partition
II	unobservable partition

Superscripts

p	pre-denitrification
n	nitrification
^	estimated

REFERENCES

Alvarez, J., and Lopez, T. (1999). Robust dynamic state estimation of nonlinear plants. *AIChE J.*, **45**(1), 107.

Aubrun, C., Therilliol, D., Harmand, J., Steyer, S.P. (2001) Software sensor design for COD estimation in an anaerobic fluidized bed reactor. *Water Sci. Tech*., 43 (7), 115.

Bernard, O., Polit, M., Hadj-Sadok, A., Pengov, M., Docahin, D. Estaben, M., Labat, P. (2001) Advanced monitoring and control of anaerobic wastewater treatment plants: Software sensors and controllers for an anaerobic digester. *Water Sci. Tech*., 43 (7), 175.

De Asís, A.J., Filho, W.M. (2000) Soft sensors development for on-line bioreactor state estimation. *Comp. Chem. Eng.*, 24, 1099.

Gomez-Quintero, C., Queinnec, I. (2001) Robust filtering for a reduced nonlinear model of an activated sludge process. *Proc. Conf. On Decision and Control 2001*.

Gomez-Quintero, C., Queinnec, I., Babary, J.P. (2000) A reduced nonlinear model for an activated sludge process. *Proc. ADCHEM 2000*, 1037.

GPS-X Technical reference manual (2001), Hydromantis Inc.

Henze, M., Leslie Grady, C.P., Gujer, W., Maris, G.V.R., Matsuo, T. (1987) Activated sludge model No. 1, I.A.W.Q. Sci. and Tech. Report No. 1, London, U.K.

Larose, A., Jorgensen, S.B. (2001). State estimation for a biological phosphorus removal process using an asymptotic observer. *Water Sci. Tech*., 43 (11), 205.

Lopez, T. (2000). Estimacion y control no lineal de reactores de copolimerizacion. Ph. D. Thesis, Universidad Autonoma Metropolitana, Mexico.

Maria, G., Maria, C., Salcedo, R., Feyo de Azevedo, S. (2000) Databank transfer-of-information, shortcut and exact estimators used in the wastewater biological treatment process identification. *Comp. Chem. Engng*., 24, 1713.

Shimizu, K. (1996). A tutorial review on bioprocess systems engineering. *Comp. Chem. Eng*., 20 (6/7), 915.

Stephanopoulos, G. (1984) *Chemical Process Control*, Prentice Hall, Englewood Cliffs, New Jersey.

Stephanopoulus, G., San K. (1984) Studies on on-line bioreactor identification. I. Theory. *Biotech. Bioeng*., 26, 1179.

EXPERIMENTAL VERIFICATION OF GAP METRIC AS A TOOL FOR MODEL SELECTION IN MULTI-LINEAR MODEL-BASED CONTROL

Omar Galán[1], Jose A. Romagnoli[2], Ahmet Palazoğlu[3], Yaman Arkun[4]

[1] ABB Australia Limited Pty, VPP9 Project, 436 Gadara Road, Tumut NSW 2720 AUSTRALIA, [2]Dept. of Chemical Engineering, The University of Sydney, Sydney, NSW, 2006, AUSTRALIA, [3]Dept. of Chemical Engineering and Materials Science, University of California, Davis, CA 95616 USA, [4]College of Engineering, Koç University, Rumelifeneri, Sarıyer, İstanbul, 80910 TURKEY

Abstract: A nonlinear system can be modeled using a set of linear models that cover the range of operation. A model-based control strategy then can be employed that uses the local models in a cooperative manner to control the nonlinear system. The decision of how many models are sufficient for effective control can be tackled by the use of the gap metric that quantifies the distance between two linear operators. A pH control experiment is used to demonstrate the effectiveness of gap metric as a tool for model selection.

Keywords: model-based control, nonlinear systems

1. INTRODUCTION

Classical linear design tools have matured to a point where one can incorporate robustness and performance requirements in a natural fashion. However for nonlinear processes strictly linear designs may not provide satisfactory performance unless they are suitably modified. One approach which tries to keep the features of linear design and at the same time account for nonlinearities is the multi-model approach for controller design (Yu *et al*., 1992; Murray-Smith and Johansen, 1997; Özkan *et al*., 2003). The key concept is to represent the nonlinear system as a combination of linear systems where classical control design techniques can be applied. The controller design based on the multi-model approach requires either simultaneous plants stabilization using a single controller, subject to performance and stability constrains (Schöming *et al*, 1995; Galán *et al*, 2000), or interpolation using model validity functions, where local controllers are selected as a function of the current state of the process (Foss *et al*, 1995; Banerjee *et al*, 1997). However, in all these approaches the question of how many and which models are required remains largely unanswered. Although it is common to use a large number of local models to improve the piece-wise linear approximation of the nonlinear system (Narendra *et al*, 1995), the optimization problem to solve the design problem becomes formidable when the number of local models is large.

We shall formulate the multi-model control problem by assuming a set of local plants and controllers that stabilize these plants and by asking the question, "Is there a reduced set of controllers, which are based on models that are 'close' in some sense?"

To determine when two systems are close to one other is a nontrivial task, and furthermore, what is meant by "close" is not entirely obvious. Since systems can be visualized as input-output operators, a natural distance concept would be the induced operator norm. Yet, the norm cannot be generalized as a distance measure (Vidyasagar, 1985). The aim of this paper is to discuss the application of a *distance measure* between systems, the so-called Gap Metric, to select a reduced set of models that contain non-redundant process information for robust stabilization of feedback systems based on multi-model controller design

2. GAP METRIC

The concept of the gap between the graphs of two linear systems goes back to Hausdorf (1935). Later the gap and other metrics were used to study how close different operators are (e.g. Newburgh (1951),

Berkson (1963)). In Zames and El-Sakkary (1980) the gap metric was used to establish a topology to quantify the tolerable uncertainties, which preserve closed loop stability. El-Sakkary (1985) shows that the gap metric is better suited to measure the distance between two linear systems than a metric based on norms. For more details, the reader is referred to these references and Galan *et al*. (2002).

Let P be a finite dimensional linear system. Its transfer function will be denoted by $\hat{P}(s)$. The transfer function $\hat{P}(s)$ can be expressed by a normalized right coprime factorization:

$$\hat{P}(s) = \hat{N}(s)\,\hat{D}^{-1}(s) \tag{1}$$

where $\hat{N}$ and $\hat{D}$ belong to the subspace of real rational functions in H_∞; $\hat{D}$ has a proper inverse, and

$$\hat{D}^*\,\hat{D} + \hat{N}^*\,\hat{N} = I \tag{2}$$

where $\hat{D}^*(s) = \hat{D}(-s)^T$. These factorizations can be computed using existing techniques (Vidyasagar, 1988).

The graph of the operator P is the subspace of $H_2 \times H_2$ (Hardy space of functions) that consists of all pairs (u, y) such that $y = P\,u$. This is expressed as

$$graph\,(P) = \begin{pmatrix} D \\ N \end{pmatrix} H_2 \equiv G H_2 \tag{3}$$

where the operator $\begin{pmatrix} D \\ N \end{pmatrix}$ is denoted by G.

Let Π_G be the orthogonal projection operator which maps any element $\{x, y\}$ in $H \times H$ to $\{u, Pu\}$ and is given by:

$$\Pi_G = G\,G^* \tag{4}$$

The calculation of the gap metric begins with two finite dimensional linear systems with the same number of inputs and outputs whose normalized coprime factorizations are given by:

$$\hat{P}_i(s) = \hat{N}_i(s)\,\hat{D}_i^{-1}(s) \tag{5}$$

and their respective "graph" operators G_i are defined as above for i=1 and 2.

It can be shown that the directed gap can be computed using the projection operators or the coprime factorizations (Georgiou, 1988):

$$\begin{aligned} \vec{\delta}(P_1, P_2) &= \left\| (I - \Pi_{G_2})\Pi_{G_1} \right\| \\ &= \inf_{Q \in H_\infty} \left\| \begin{pmatrix} D_1 \\ N_1 \end{pmatrix} - \begin{pmatrix} D_2 \\ N_2 \end{pmatrix} Q \right\|_\infty \end{aligned} \tag{6}$$

Definition 2 (Georgiou, 1988): The gap between two systems P_1 and P_2 is given by:

$$\delta(P_1, P_2) = \max\left\{ \vec{\delta}(P_1, P_2),\, \vec{\delta}(P_2, P_1) \right\}$$

and using (6) one gets

$$\max \left\{ \begin{array}{l} \inf\limits_{Q \in H_\infty} \left\| \begin{pmatrix} D_1 \\ N_1 \end{pmatrix} - \begin{pmatrix} D_2 \\ N_2 \end{pmatrix} Q \right\|_\infty, \\ \inf\limits_{Q \in H_\infty} \left\| \begin{pmatrix} D_2 \\ N_2 \end{pmatrix} - \begin{pmatrix} D_1 \\ N_1 \end{pmatrix} Q \right\| \end{array} \right\} \tag{7}$$

Properties of the gap:

1. The gap defines a metric on the space of (possibly unstable) linear systems.
2. $0 \le \delta(P_1, P_2) \le 1$

The metric defines a notion of distance in the space of (possibly unstable) linear systems, which do not assume that plants have the same number of poles in the RHP.

The computation of the *gap* involves solving two-block H_∞ problems (7). In our examples, we used MATLAB μ-Synthesis Toolbox to compute the gap.

If the gap metric is close to zero, it indicates that the distance between two systems is 'close'. If, on the other hand, the gap is closer to 1; then, the two systems' dynamic behaviors are 'apart'. In the following experimental study, we use the gap metric to distinguish between models in a given set. We use the gap analysis to select appropriate linear models to control a pH neutralization system using a multi-linear controller.

3. EXPERIMENTAL STUDY

The model of the process for pH neutralization is taken from the paper by Galán *et al*. (2000). Based on that model, first-order transfer function models are derived for five distinct operating regions in the steady-state map (Fig. 1).

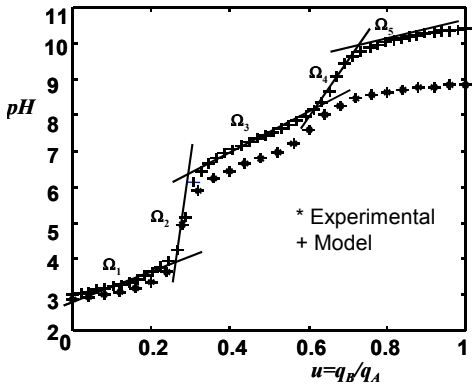

Fig. 1. The steady-state map of the process and the model prediction, indicating five regions for local linear models.

Table 2 shows the gap metric between the pairs of five linear models representing the operating range for the nonlinear system (Fig. 1). The numbers suggest that model subsets $\Omega_{HS} = \{\Omega_2, \Omega_4\}$ and $\Omega_{LS} = \{\Omega_1, \Omega_3, \Omega_5\}$ are closer to being "different" while the members in each subset are closer to being "similar." Model 2 is considered different than

models 1, 3 and 5 as the gap metric is around 1, but close to model 4. This similarity between models 2 and 4 can be explained physically by the fact that those models represent high sensitivity regions "Ω_{HS}", that is, regions with a steep slope (Fig. 1). It contrasts with models 1, 3 and 5, which represent the low sensitivity regions "Ω_{LS}".

Table 2. Distance between Linear Models Using Gap Metric.

δ	1	2	3	4	5
1	0.0000	0.9331	0.2561	0.8050	0.2619
2	0.9331	0.0000	0.8885	0.5137	0.9515
3	0.2561	0.8885	0.0000	0.6892	0.4183
4	0.8050	0.5137	0.6892	0.0000	0.8567
5	0.2619	0.9515	0.4183	0.8567	0.0000

3.1 Controller Design

Consider a set of *N* local linear models that, in combination, describe the behavior of a nonlinear system in a pre-defined operating range. The key issue is how one implements the multi-model control scheme with a set of local controllers that are derived using the local models. For this example, the controllers for different local operating regions are *combined* to form a complete control system, using membership functions to create a transition region in the measured variable "*y*" (de Silva and MacFarlane, 1989).

$$\hat{\phi}_p(y) = \frac{\phi_p}{\sum_{p=1}^{n} \phi_p} \tag{8}$$

The subscript *p* represents the p^{th} member of a set of *N* controllers. Given the output variable *y*, the membership function returns a number between zero and one indicating the level of contribution of the local controller at that value of the output. We define the distribution function for a local controller,

$$\phi_p(y) = \exp\left[-\frac{1}{2}\left(\frac{y - \bar{y}_p}{\sigma_p} \right)^2 \right] \tag{9}$$

where $\bar{y}_p$ and σ_p are the mean and the standard deviation related to the model "*p*", respectively. The desired contribution of combined controllers on the control signal can be represented as a function of the membership functions:

$$u(t) = \sum_{p=1}^{N} \hat{\phi}_p u_p(t) \tag{10}$$

The block diagram for the local controllers is given in Figure 2. Given a SISO plant $\hat{g}_p(s)$, a controller $\hat{k}_p(s)$ is designed such that the basic requirements of stability, performance and robustness are satisfied (Doyle et al., 1992). This can be done by finding a robust controller that minimizes the mixed-sensitivity criterion (Skogestad and Postletwaite, 1996),

$$J = \sup_{\omega} \begin{vmatrix} \hat{w}_e(s)\hat{S}_p(s) \\ \hat{w}_u(s)\hat{k}_p(s)\hat{S}_p(s) \\ \hat{w}_y(s)\hat{T}_p(s) \end{vmatrix} = \left\| \begin{matrix} \hat{w}_e(s)\hat{S}_p(s) \\ \hat{w}_u(s)\hat{k}_p(s)\hat{S}_p(s) \\ \hat{w}_y(s)\hat{T}_p(s) \end{matrix} \right\|_{\infty} \tag{11}$$

Note that $\hat{S}_p(s)$, and $\hat{T}_p(s)$ are the local sensitivity and complementary sensitivity functions respectively. Accordingly, $\hat{w}_e$, $\hat{w}_u$ and $\hat{w}_y$ are the corresponding weight (penalty) functions chosen to shape the closed-loop performance and robustness behavior.

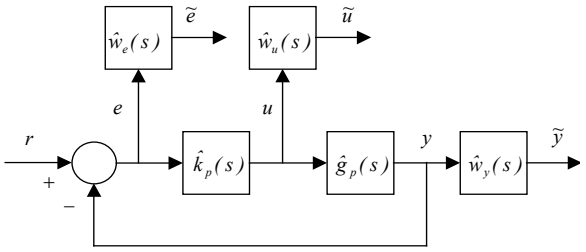

Fig. 2. Block diagram for the local closed-loop system.

3.2 Experimental verification

To study the closed-loop performance of these controllers based on a subset of models, real-time experiments are performed. An acid stream (HCl solution) and an alkaline stream (NaOH and $NaHCO_3$ solution) are fed to a 2.5-liter constant volume, well-mixed tank, where the pH is measured through a sensor located directly in the tank. The control objective is to drive the system to different pH conditions (tracking control) by manipulating the alkaline stream flowrate.

Figure 3 shows the tracking performance when all five models are included. The response is generally acceptable, but the aggressive behavior around pH=5 (region 2) is noted. We can compare this performance with the case where only three models (from Ω_{LS}) are included. Figure 4 shows that there is clearly a loss of performance, especially around region 2. This validates what we have seen before in the gap metric analysis, as these models are not sufficiently descriptive of the whole operating region.

When only two models 1 and 2 or 2 and 3 are used in combination (one model from Ω_{LS} and one model from Ω_{HS}), the results are given in Figs. 5 and 6, respectively

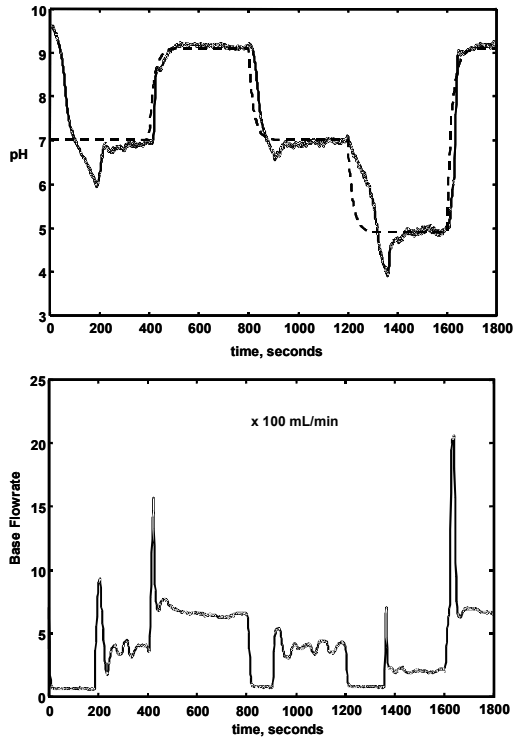

Fig. 3. Tracking performance when all five models used.

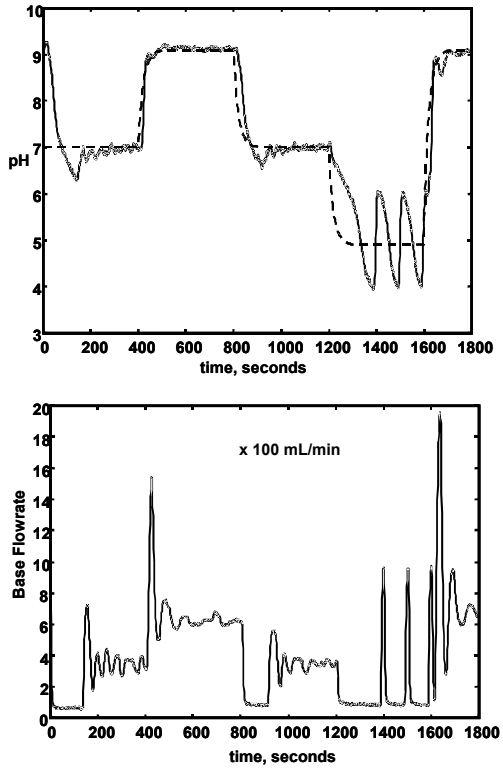

Fig. 4. Tracking performance when only models from the set Ω_{LS} are used.

The responses are quite similar to the one obtained by using all five models as models in region 2 and 4 sufficiently explain the dynamics within the operating region. In fact, the control action appears to be much smoother when only two models are considered. The results also indicate that the first combination (1, 2) exhibits some degradation in performance while the second (2, 3) offers a more satisfactory tracking behavior (especially in the control action).

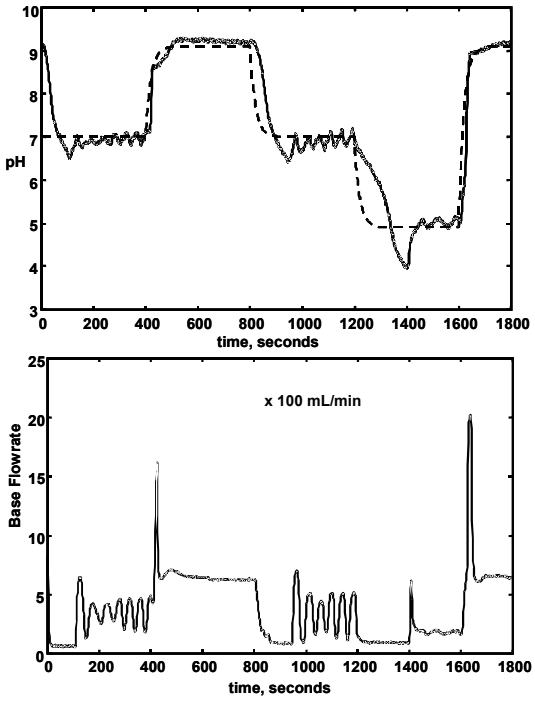

Fig. 5. Tracking performance when two models used, one from each sensitivity region.

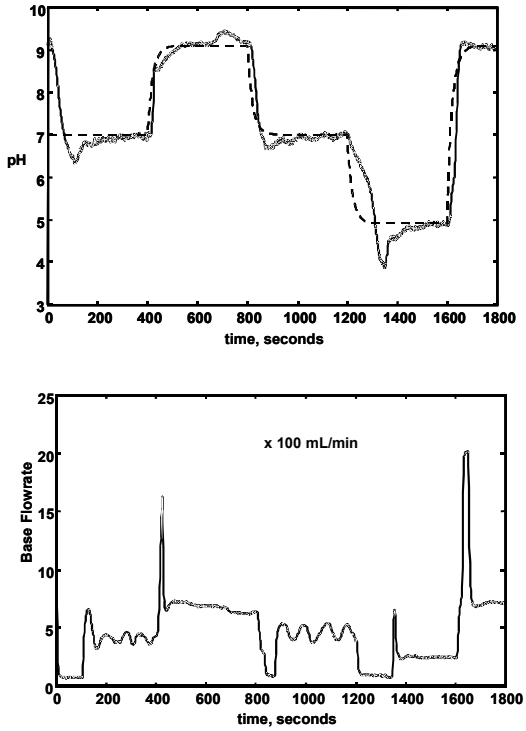

Fig. 6. Tracking performance when two models used, one from each sensitivity region.

CONCLUSIONS

The results of the case study using gap metric, as a measure of the distance between two linear plants, suggests the potential for a rigorous measure to evaluate the number of models in multi-linear model-based control. For the case of pH neutralization where one intuitively would use five models to cover the pH range between 3 and 10, we have shown that two models may be sufficient to guarantee satisfactory closed-loop performance.

Acknowledgements: A grant from the Australian Research Council (ARC-A89906571) is gratefully acknowledged.

REFERENCES

Banerjee, A, Arkun, Y., Ogunnaike, B., Pearson, R., (1997). "Estimation of Nonlinear Systems Using Linear Multiple Models," *AIChE J*., **43**, 1204-1226.

Berkson, E., (1963). "Some Metrics on the Subspaces of a Banach Space," *Pacific J. Math*, **13**, 7-22.

de Silva, C.W., and MacFarlane, A.G.J., (1989). *Knowledge-Based Control with Application to Robots*, Springer-Verlag, NY.

Doyle, J.C., Francis, B.A. and Tannenbaum, A.R., (1992). *Feedback Control Theory*, Macmillan, New York, NY.

El-Sakkary, A., 1985, "The Gap Metric: Robustness of Stabilization of Feedback Systems," *IEEE Trans. on Automatic Control*, **AC-30**, 240-247.

Foss, B.A., Johansen, T.A. and Sorensen, A.V., 1995, "Nonlinear Predictive Control Using Local Models - Applied to a Batch Fermentation Process," *Control Eng. Practice*, **3**, 389-396.

Galán, O., Palazoglu, A. and Romagnoli, J. A., 2000, "Robust H_∞ Control for Nonlinear Plants Based on Multi Linear Models – An Application to a Bench Scale pH Neutralization Reactor," *Chem. Eng. Sci*., **55**, 4435-4450.

Galán, O., Romagnoli, J. A., Palazoglu, A. and Arkun, Y. (2002). "The Gap Metric Concept and Implications for Multi-Linear Model-Based Controller Design," *Ind. & Engg Chem., Research*, submitted.

Georgiou, T.T., 1988, "On the Computation of the Gap Metric," *Systems & Control Letters*, **11**, 253-257.

Hausdorff, F.,(1935). *Mengenlehre,* Berlin: Leipzig.

Murray-Smith, R., and Johansen, T.A. (eds.), 1997, *Multiple Model Approaches to Modeling and Control*, Taylor & Francis, London, England.

Narendra, K.S., Balakrishnan, J. and Ciliz, M.K., 1995, "Adaptation and Learning Using Multiple Models, Switching and Tuning," *IEEE Control Syst. Magazine*, **15**, 37-51.

Newburgh, J. D., 1951, "A Topology for Closed Operators," *Ann. Math*., **53**, 250-255.

Özkan, L., Kothare, M.V., and Georgakis, C., 2003, "Control of a Solution Copolymerization Reactor Using Multi-Model Predictive Control," *Chem. Eng. Sci*., in press.

Schöming, E., Sznaier, M. and Ly, U., 1995, "Mixed H_2/H_∞: Control of Multimodel Plants," *J. Guidance, Control and Dynamics*, **18**, 525-531.

Skogestad, S. and Postlethwaite, I., 1996, *Multivariable Feedback Control*, Wiley, New York, NY.

Vidyasagar, M., 1985, *Control System Synthesis: A Factorization Approach*, MIT Press, Cambridge, MA.

Vidyasagar, M., 1988, "Normalized Coprime Factorizations for Nonstrictly Proper Systems," *IEEE Trans. Automat. Control*, **33**, 300-301.

Yu, C., Roy, R.J., Kaufman, H., and Bequette, B.W., 1992, "Multiple-Model Adaptive Predictive Control of Mean Arterial Pressure and Cardiac Output," *IEEE Trans. Biomed.Eng.,* 39, 765-778.

Zames, G. and El-Sakkary, A.K., 1980, "Unstable Systems and Feedback: The Gap Metric," Proceedings of the Allerton Conf., 380-385.

BAYESIAN ESTIMATION OF UNCONSTRAINED NONLINEAR DYNAMIC SYSTEMS

Wen-shiang Chen [*] **Bhavik R. Bakshi** [*] **Prem K. Goel** [**]
Sridhar Ungarala [***]

[*] *Dept. Chem. Eng., The Ohio State University*
Columbus, OH 43210, USA
[**] *Dept. Statistics, The Ohio State University*
Columbus, OH 43210, USA
[***] *Dept. Chem. Eng., Cleveland State University*
Cleveland, OH 44115, USA

Abstract: Accurate estimation of state variables and model parameters is essential for efficient process operation. The Bayesian formulation of the estimation problem suggests a general solution for nonlinear systems. However, a practically feasible implementation of the solution has not been available until recently. Most existing methods have had to rely on simplifying assumptions to obtain an approximate solution. For example, extended Kalman filtering estimates the system state by linearizing the nonlinear model and assuming Gaussian distributions for all random variables. Moving horizon estimation assumes Gaussian or other fixed-shape distributions to formulate a constrained least-squares optimization problem. In this paper, Bayesian estimation is implemented by sequential Monte Carlo sampling. This approach can represent non-Gaussian distributions accurately and efficiently with minimum assumptions and computes moments by Monte Carlo integration. The features of the Monte Carlo approach are demonstrated by application to a state estimation case study of a CSTR process. The proposed method exhibits 78% improvement in estimation error and takes 95% less time than moving horizon estimation to solve the problem.

Keywords: Bayesian estimation, Sequential Monte Carlo sampling

1. INTRODUCTION

Efficient operation of chemical and manufacturing processes relies on cleaning or rectification of measured data and estimation of unknown quantities. Data rectification and estimation form the foundation for process operation tasks such as process control, fault detection and diagnosis, real-time estimation, process monitoring, and process scale-up. Due to the importance of these tasks, many methods have been developed under the names of data rectification, data reconciliation, and state and parameter estimation (Kramer and Mah, 1994; Robertson *et al.*, 1996).

In general, the goal of estimation may be expressed as follows. Given measurements $y_{1:k} = \{y_1, y_2, \ldots, y_k\}$, process models, and the distribution of the initial condition $p(x_0)$, determine the current state, x_k. Process models may be expressed as follows,

$$x_k = f_{k-1}(x_{k-1}, \omega_{k-1}) \tag{1}$$

$$y_k = h_k(x_k, \nu_k) \tag{2}$$

where $x_k \in \Re^{n_x}$ is the state vector and $f_k : \Re^{n_x} \times \Re^{n_\omega} \rightarrow \Re^{n_x}$ is the system equation. Measurements, $y_k \in \Re^{n_y}$, are related to the state vector through the measurement equation, $h_k : \Re^{n_x} \times \Re^{n_\nu} \rightarrow \Re^{n_y}$.

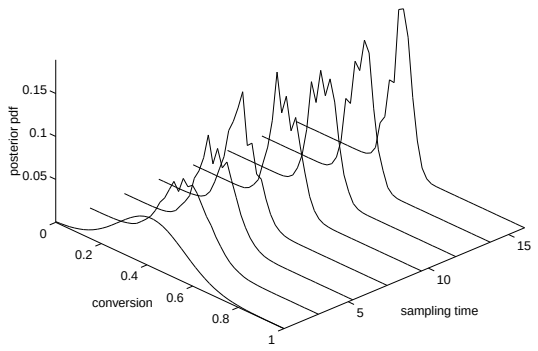

Fig. 1. Evolution of the conditional distribution of concentration in a CSTR.

Significant efforts have been focused on methods for rectification and estimation in nonlinear dynamic systems, with and without constraints (Jang *et al.*, 1986; Tjoa and Biegler, 1991; Liebman *et al.*, 1992; Robertson *et al.*, 1996; Rao and Rawlings, 2002). However, all the existing methods rely on simplifying assumptions about the nature of the model or the probability distributions of the underlying variables to obtain a tractable optimization problem. A popular assumption is that the distribution of the variables to be estimated is Gaussian or of a fixed, time-invariant shape. The crudeness of this assumption is depicted in Figure 1, which shows the conditional distribution over time for a popular continuously stirred tank reactor (CSTR) case study (Jang *et al.*, 1986; Liebman *et al.*, 1992; Robertson *et al.*, 1996). The multi-modal, skewed and time-varying nature of these distributions indicates that approximating them by Gaussian or other fixed-shape distributions can be grossly incorrect. The approximations may also fail in the presence of constraints, since constraints may require the probability of some variables to be zero in regions where the constraint is violated (Robertson *et al.*, 1996; Rao and Rawlings, 2000; Chen *et al.*, 2002; Robertson and Lee, 2002). Nevertheless, these assumptions are popular since they permit existing methods to solve a convenient problem instead of the actual estimation problem. These shortcomings of existing methods and the challenges in obtaining the Bayesian solution are well-known and have been widely recognized (Robertson *et al.*, 1996; Rao and Rawlings, 2000; Robertson and Lee, 2002).

The Bayesian formulation provides a solution to the actual estimation problem without necessitating invalid assumptions. However, until recently, the implementation of the Bayesian solution was considered impractical due to its heavy computational demand. Recently, efficient algorithms based on Monte Carlo sampling along with increasing computational ability are making Bayesian estimation feasible for real problems (Malakoff, 1999).

This paper introduces a computationally efficient approach for data rectification of nonlinear dynamic systems based on a statistically rigorous Bayesian formulation. This approach relies on sequential Monte Carlo (SMC) sampling to maximize the use of data and knowledge to obtain the Bayesian solution without relying on assumptions about the nature of the errors, model and underlying variables. The main contributions of this paper are to introduce SMC methods into process engineering, and compare their performance with currently popular methods. This work also indicates that for many nonlinear dynamic systems, Gaussian approximations are not necessarily more computationally efficient, and may be less accurate.

In the following sections, a Bayesian view of existing methods is first discussed. After that, a brief introduction on Monte Carlo sampling is provided. Then the detail of the implementation of the proposed approach is provided and discussed. Performance of the proposed approach is compared with that of existing approaches in the case study section.

2. BAYESIAN VIEW OF EXISTING METHODS

2.1 Background

Bayesian estimation maximizes the use of all available information and can handle all types of errors, models and constraints. In addition, Bayesian estimation finds the distribution of states, which can provide uncertainty information. For dynamic systems, recursive Bayesian estimation may be represented as follows (Ho and Lee, 1964),

$$p(x_k|y_{1:k}) = \frac{p(y_k|x_k)\ p(x_k|y_{1:k-1})}{p(y_k|y_{1:k-1})}, \qquad (3)$$

where the posterior distribution, $p(x_k|y_{1:k})$, combines information from current measurement via the likelihood function $p(y_k|x_k)$, and past information using the prior distribution $p(x_k|y_{1:k-1})$. The denominator is a normalizing constant. Each term in Equation (3) may be obtained as follows. For the second term in the numerator,

$$p(x_k|y_{1:k-1}) = \int p(x_k|x_{k-1})\ p(x_{k-1}|y_{1:k-1})\ dx_{k-1} \quad (4)$$

where $p(x_{k-1}|y_{1:k-1})$ is the posterior of time step $k-1$. $p(x_k|x_{k-1})$ may be further manipulated as the following equation.

$$p(x_k|x_{k-1}) = \int \delta(x_k - f_{k-1}(x_{k-1}, \omega_{k-1}))\ p(\omega_{k-1})\ d\omega_{k-1} \quad (5)$$

Similarly, $p(y_k|x_k)$ in Equation (3) may be found as follows,

$$p(y_k|x_k) = \int \delta(y_k - h_k(x_k, \nu_k))\ p(\nu_k)\ d\nu_k \quad (6)$$

In general, there is no closed-form solution for Equation (3) to Equation (6) except for linear Gaussian systems. Even when the functionality of the distributions is known, the calculation of their moments needs multi-dimensional integrations, which may be computationally expensive. Therefore, it is not surprising to see that methods based on simplification have been popular in the past. Many existing approaches may be interpreted as approximate Bayesian estimation. These methods tend to simplify the real problem so that a convenient solution may be found. In the following section, an overview of existing approaches for estimation from the view point of Bayesian estimation is provided. These methods may be categorized by how posterior distributions are propagated over time and their moments are computed. In the following sections, two main categories are discussed, Gaussian approximation and direct integration.

2.2 Gaussian approximation

Gaussian distributions are convenient since only two parameters, mean and variance, are required to describe a whole distribution. Although, the assumption of Gaussian prior is suitable in linear systems, it can be easily violated in nonlinear dynamic systems (Chen *et al.*, 2003). The assumption of Gaussian prior worsens when process constraints are enforced and results in truncated distributions (Chen *et al.*, 2002; Robertson and Lee, 2002). Even though Gaussian approximation may not be a valid assumption for nonlinear dynamic systems, approaches based on this assumption are popular for its simplicity. Two variations of Gaussian approximation namely, extended Kalman filtering (EKF) and moving-horizon estimation (MHE), are discussed here.

EKF is an extension of Kalman filtering to nonlinear dynamic systems. Kalman filtering is the optimal estimator for linear dynamic systems with Gaussian prior and additive independent and identically distributed (iid) Gaussian noise without constraints. The filter is optimal with respect to minimum variance criterion. In addition, Kalman filtering has a closed-form solution that makes estimation extremely efficient. The natural extension of Kalman filtering into nonlinear dynamic systems is to linearize nonlinear process models so that the same solution strategy for Kalman filtering can be applied. In doing so, EKF inherits all assumptions made by Kalman filtering, including Gaussian prior and noise. EKF is favored for its simplicity and efficiency, but the filter may diverge from the true state and does not necessarily satisfy process constraints. Further discussion of Kalman filtering and EKF can be found in Jazwinski (1970) and Maybeck (1979).

Efforts have been made to avoid divergence of EKF. One suggestion is to retain higher order terms of Taylor's expansion so that more accurate local linearization may be achieved. Divergence due to poor approximation may be reduced, but new complexity arises in determining the "right" highest term to keep, which may not be a trivial task.

MHE also relies on the assumption of Gaussian prior and noise so that a least-squares estimation (LSE) may be found (Robertson *et al.*, 1996). Unlike EKF, MHE can enforce constraints which is equivalent to using truncated Gaussian prior (Robertson and Lee, 2002). MHE also needs selection of a proper window size to compromise between the accuracy of batch-processed least-squares estimation and the efficiency of solving a smaller problem. Furthermore, MHE relies on constrained nonlinear programming, which is usually computationally expensive and it becomes difficult to asses its statistical properties. Even in cases where Gaussian approximation may be an acceptable assumption, the proposed Bayesian approach usually has better accuracy and tends to require less computation than approaches like MHE.

2.3 Direct Numerical Integration

Methods in this category represent the distribution of interest over a grid of points in state space. Once a suitable grid is identified, numerical integration may be used to compute the moments of the distribution. This approach can provide the exact solution if the state space is discrete and finite. In most cases, the number of states is not finite, and selecting the grid can be quite challenging since a fine grid is computationally expensive, while a coarse grid may be inaccurate. Many variations have been developed based on fixed or adaptive grids. Approaches such as cell-to-cell mapping and Hidden Markov Models may be considered to be special cases of this approach. While this approach has become more feasible with advances in computing, it is still too expensive for solving multidimensional problems.

3. MONTE CARLO SAMPLING

Monte Carlo sampling based approaches use samples to approximate a distribution as,

$$p(x) \approx \sum_{i=1}^{N} q(i)\ \delta(x - x(i)) \tag{7}$$

where $x(i)$ is the i-th sample that represents the distribution. The coefficient, $q(i)$, is the probability mass associated with each sample. $q(i)$ equals $1/N$ for $x(i)$ randomly drawn from $p(x)$. By the law of large numbers, as the number of samples goes to infinity, the approximation converges to the exact distribution.

Integration based on Monte Carlo sampling may be expressed as,

$$E[\phi(x)] = \int \phi(x)\ p(x)dx$$
$$\approx \frac{1}{N}\sum_{i=1}^{N} \phi(x(i)) \quad (8)$$

where $x(i)$ again is the i-th sample drawn from the distribution $p(x)$.

Estimation based on Equation (8) relies on samples drawn from the known distribution, $p(x)$. In real problems, $p(x)$ may not be readily available for sampling, but its value can be evaluated for a given sample of $x(i)$. This leads to the use of importance sampling.

3.1 Importance Sampling

Importance sampling relaxes the requirement of generating samples from the true distribution for estimating Equation (8). Instead, it relies on drawing samples from a convenient distribution, $\pi(x)$, called the importance function. Equation (8) may be reformulated as,

$$E[\phi(x)] = \int \phi(x)\ p(x)\ dx$$
$$= \int \frac{\phi(x)\ p(x)}{\pi(x)}\ \pi(x)\ dx$$
$$\approx \frac{1}{N}\sum_{i=1}^{N} q(i) \quad (9)$$

where $q(i) = \frac{\phi(x(i))\ p(x(i))}{\pi(x(i))}$ is the weight function. It should be noted here that $x(i)$ are samples drawn from $\pi(x)$ instead of $p(x)$. Convergence is almost guaranteed under minimal assumptions, such as, the support of $\pi(x)$, contains the support of $p(x)$ (Geweke, 1989).

For dynamic systems, Monte Carlo sampling techniques can be implemented recursively when new measurements arrive, and is termed sequential Monte Carlo sampling. The following section describes a Bayesian estimation approach based on sequential Monte Carlo sampling.

4. SEQUENTIAL MONTE CARLO SAMPLING FOR BAYESIAN ESTIMATION

The goal of Bayesian estimation is to obtain the posterior accurately and efficiently. The algorithm for recursive Bayesian estimation may be visualized as in Figure 2. Information in previous measurements up to time $k-1$ is captured by the posterior distribution, $p(x_{k-1}|y_{1:k-1})$. Prediction of distribution of the current state is implemented by utilizing Equations (4) and (5). Information in current measurement is represented as the likelihood function based on Equation (6). The posterior can then be found by combining previous and current information by Equation (3).

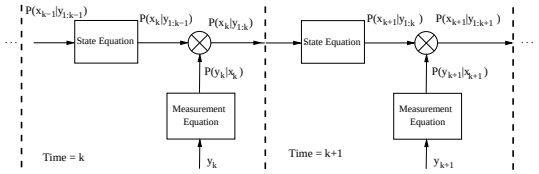

Fig. 2. Algorithm of recursive Bayesian estimation.

The application of sequential Monte Carlo sampling may be described as finding the appropriate weight for each sample so that posterior distribution may be approximated by the samples as in Equation (7). The algorithm may be represented in pseudo-code as follows (Arulampalam *et al.*, 2002):

- FOR times $k = 1,2,3,\ldots$
  - FOR samples $i = 1,2,3,\ldots,N$
    - Draw sample, $x_k(i)$ from an importance function, $\pi(x_k(i)|x_{k-1}(i),y_k)$
    - Assign a weight to $x_k(i)$, $q_k^*(i)$
  - END FOR
  - Normalize $q_k^*(i)$ to find $q_k(i)$
- END FOR

where

$$q_k^*(i) = q_{k-1}(i)\frac{p(y_k|x_k(i))\ p(x_k(i)|x_{k-1}(i))}{\pi(x_k(i)|x_{k-1}(i),y_k)} \quad (10)$$

can be found based on Equations (3) to (6).

A convenient choice of importance function is to use samples of prior as the importance function (Gordon *et al.*, 1993),

$$\pi(x_k(i)|x_{k-1}(i),y_k) = p(x_k(i)|x_{k-1}(i)) \quad (11)$$

This choice simplifies Equation (10) to

$$q_k^*(i) = q_{k-1}(i)\ p(y_k|x_k(i)) \quad (12)$$

More sophisticated choice of importance functions is expected to improve the robustness of SMC (Doucet *et al.*, 2000; Cheng and Druzdzel, 2000). In the next section, one practical issue in applying the proposed approach to estimation problem, known as degeneracy, is discussed.

4.1 Degeneracy

Degeneracy is a phenomenon where the weights of most samples become insignificant after a few time steps. Therefore, computation may be wasted on samples with little or no importance to the distribution. In addition, since estimation is mainly determined by a few samples, approximation of distributions may result in spurious spikes.

Degeneracy may be reduced by choosing importance functions that minimize the variance of sample weights. $\pi(x_k(i)|x_{k-1}(i),y_k)$, has been suggested as one such importance function (Doucet *et al.*, 2000).

Cheng and Druzdzel (2000) have also suggested an adaptive algorithm for finding importance functions, which is more robust when unlikely measurements occur. This approach to updating importance functions may help in reducing degeneracy since it tends to become severe when the measurement and prediction do not match each other. Markov chain Monte Carlo (MCMC) sampling which may be interpreted as iterative process of finding importance functions may also reduce degeneracy (Andrieu *et al.*, 2003).

Degeneracy can also be reduced by resampling. Resampling involves drawing samples from the weighted sample pool according to samples' weights. Samples with insignificant weights are less likely to be resampled. Further discussion of resampling can be found in Chen *et al.* (2003).

5. CASE STUDY

A typical chemical engineering problem, an adiabatic CSTR, is studied. Governing equations for this CSTR case study are provided as follows (Jang *et al.*, 1986; Liebman *et al.*, 1992; Henson and Seborg, 1997; Robertson and Lee, 1995).

$$\frac{dC}{dt} = \frac{q}{V}(C_0 - C) - k\,C\,e^{\frac{-E_A}{T}} \tag{13}$$

$$\frac{dT}{dt} = \frac{q}{V}(T_0 - T) - \frac{\Delta H}{\rho\,C_p}\,k\,C\,e^{\frac{-E_A}{T}} - \frac{U\,A}{\rho\,C_p\,V}(T - T_c) \tag{14}$$

Operating conditions and simulation parameters can be found in Henson and Seborg (1997). Three estimation approaches are compared in this case study, including EKF, MHE and SMC. MHE is implemented with horizon width 2, while 500 samples are used at each time step for SMC.

Figure 3 displays the evolution of posterior distribution of concentration into skewed non-Gaussian distributions, approximated by SMC with 5000 samples. Figure 4 shows the multi-modal posterior distributions.

Performance of these three methods is compared based on mean-squares error (MSE) and CPU time required for estimation (in units of CPU seconds per time step). Results provided in Table 1 are based on 100 realizations of simulation, and in each realization, 1600 measurements are rectified. CPU time is based on a personal computer with Pentium 400 MHz and 128MB RAM.

The proposed approach, SMC, exhibits significant improvement over both EKF and MHE in estimation error. SMC shows 78% improvement over MHE, and confirms the expectation that without making invalid assumptions on distributions, estimation by SMC is more accurate. Although MHE has better estimation results than EKF, it requires 19 times more computational effort than SMC. Verification of this result using customized MHE is also under progress. This result indicates that methods based on Gaussian approximation need not be computationally more efficient than methods based on other distributions.

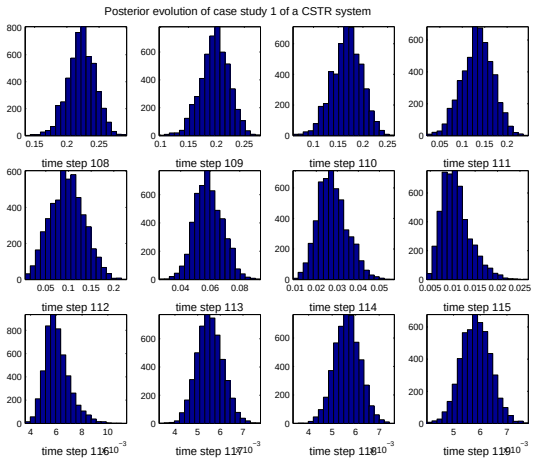

Fig. 3. Skewed posterior distributions: time step 109 and 115.

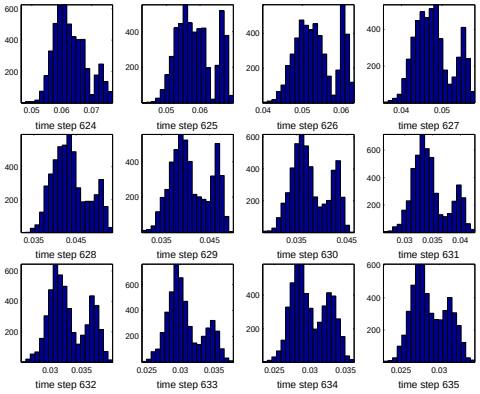

Fig. 4. Multi-modal posterior distributions.

Table 1. Average Mean-Squares Error and CPU time for CSTR Case Study

	EKF	MHE	SMC
MSE	0.13 ± 0.05	0.09 ± 0.04	0.02 ± 0.01
CPU	0.002 ± 0.00	0.58 ± 0.22	0.03 ± 0.01
Parameters		width$= 2$	$N = 500$

6. CONCLUSIONS

In this paper, a novel estimation approach based on a rigorous Bayesian formulation is introduced. The proposed approach uses sequential Monte Carlo sampling to propagate state information recursively. The Monte Carlo approach avoids direct numerical integration for computing the moments of state probability distributions. SMC benefits from not making invalid assumptions, such as Gaussian or other fixed-shape prior and

noise, compared with most existing approaches. SMC is shown to outperform EKF by a wide margin in accuracy. It outperforms MHE in terms of accuracy and computation time even when the distributions satisfy the MHE assumption of being Gaussian. The benefits of this proposed approach are expected to be even more significant for constrained nonlinear dynamic systems (Chen *et al.*, 2002). The proposed approach can handle all types of errors, models and constraints with the same solution strategy.

7. ACKNOWLEDGMENTS

Financial support from the National Science Foundation (CTS-9733627) is gratefully acknowledged.

REFERENCES

Andrieu, Christophe, Nando de Freitas, Arnaud Doucet and Michael Jordan (2003). An introduction to MCMC for machine learning. *Machine Learning* **50**(1-2), 5–43.

Arulampalam, M. Sanjeev, Simon Maskell, Neil Gordon and Tim Clapp (2002). A tutorial on particle filters for online nonlinear/non-Gaussian Bayesian tracking. *IEEE Transactions on Signal Processing* **50**(2), 174–188.

Chen, Wen-shiang, Bhavik R. Bakshi, Prem K. Goel and Sridhar Ungarala (2002). Bayesian estimation of nonlinear dynamic systems - dealing with constraints and non-Gaussian errors. In: *AIChE Annual Meeting, Indianapolis, IN*. `http://www.che.eng.ohio-state.edu/~chenwe/publications/aiche2002_chen.pdf`.

Chen, Wen-shiang, Bhavik R. Bakshi, Prem K. Goel and Sridhar Ungarala (2003). Bayesian estimation of unconstrained nonlinear dynamic systems via sequential Monte Carlo sampling. Technical report. Department of Chemical Engineering, The Ohio State University. `http://www.che.eng.ohio-state.edu/~chenwe/publications/BayMC_Intro.pdf`.

Cheng, Jian and Marek J. Druzdzel (2000). Aisbn: An adaptive importance sampling algorithm for evidential reasoning in large bayesian networks. *Journal of Artificial Intelligence Research* **13**, 155–188.

Doucet, Arnaud, Simon Godsill and Christophe Andrieu (2000). On sequential Monte Carlo sampling methods for Bayesian filtering. *Statistics and Computing* **10**, 197–208.

Geweke, John (1989). Bayesian inference in econometric models using Monte Carlo integration. *Econometrica* **57**(6), 1317–1339.

Gordon, N. J. and D. J. Salmond and A. F. M. Smith (1993). Novel approach to nonlinear/non-Gaussian Bayesian state estimation. *IEE Proceedings-F* **140**(2), 107–113.

Henson, Michael A. and Dale E. Seborg (1997). *Nonlinear Process Control*. Upper Saddle River, New Jersey; Prentice Hall PTR.

Ho, Y. C. and R. C. K. Lee (1964). A Bayesian approach to problems in stochastic estimation and control. *IEEE Transactions on Automatic Control* pp. 333–339.

Jang, Shi-Shang, Babu Joseph and Hiro Mukai (1986). Comparison of two approaches to on-line parameter and state estimation of nonlinear systems. *Ind. Eng. Chem. Process Des. Dev.* **25**, 809–814.

Jazwinski, Andrew H. (1970). *Stochastic Processes and filtering theory*. Academic Press, New York.

Kramer, M. A. and R. S. H. Mah (1994). Model-based monitoring. In: *Proceedings of the International Conference on Foundations of Computer Aided Process Operations, CACHE, Austin, TX* (D. Rippin, J. Hale and J. Davis, Eds.).

Liebman, M. J., T. F. Edgar and L. S. Lasdon (1992). Efficient data reconciliation and estimation for dynamic processes using nonlinear programming techniques. *Computers and Chemical Engineering* **16**(10/11), 963–986.

Malakoff, David (1999). Bayes offers a 'new way' to make sense of numbers. *Science* **286**, 1460–1464.

Maybeck, Peter S. (1979). *Stochastic Models, estimation and control*. Academic Press, New York.

Rao, Christopher V. and James B. Rawlings (2000). *Nonlinear moving horizon state estimation*. Nonlinear Model Predictive Control. Birkhauser.

Rao, Christopher V. and James B. Rawlings (2002). Constrained process monitoring: Moving-horizon approach. *AIChE Journal* **48**(1), 97–109.

Robertson, Douglas G. and Jay H. Lee (1995). A least squares formulation for state estimation. *J. Proc. Cont.* **5**(4), 291–299.

Robertson, Douglas G. and Jay H. Lee (2002). On the use of constraints in least squares estimation and control. *Automatica* **38**, 1113–1123.

Robertson, Douglas G., Jay H. Lee and James B. Rawlings (1996). A moving horizon-based approach for least-squares estimation. *AIChE Journal* **42**(8), 2209–2224.

Tjoa, I. B. and L. T. Biegler (1991). Simultaneous strategies for data reconciliation and gross error detection of nonlinear systems. *Computers and Chemical Engineering* **15**(10), 679–690.

Multivariate Analysis of Process Data using Robust Statistical Analysis and Variable Selection

Leo H. Chiang, Randy J. Pell, and Mary Beth Seasholtz

The Dow Chemical Company
Analytical Sciences Laboratory
Corporate R&D
1897 Building
Midland, MI 48667
U.S.A.

Abstract: Historical plant data are useful in developing multivariate statistical models for on-line process monitoring, soft sensors, and process troubleshooting. For the first two purposes, historical data are used to build a model to capture the normal characteristics of the process. However, the presence of outliers can adversely affect the model. Various robust statistical techniques are investigated in this paper for outlier identification. For process troubleshooting and fault identification, it is crucial to identify the key process variables that are associated with the root causes. Genetic algorithms (GA) are incorporated with Fisher discriminant analysis (FDA) for this purpose. These techniques have been successfully applied at The Dow Chemical Company.

Keywords: Fault identification, robust estimation, genetic algorithms, data processing, bad data identification

1. INTRODUCTION

Process data are rapidly collected and stored for the chemical industry. These historical data are highly useful in developing multivariate statistical models such as principal component analysis (PCA) or partial least squares (PLS) for on-line process monitoring. One important step in applying these techniques is to extract the normal data for the off-line model building phase. Historical databases contain data from normal operating conditions, faulty conditions, various operating modes, startup periods, and shutdown periods. The presence of outliers further complicates the task of identifying the normal data. Outliers can disrupt the correlation structure of the PCA or PLS model and the result will be a model that does not accurately represent the process. To extract representative normal data, several outlier detection algorithms such as resampling by half-means (RHM), smallest half volume (SHV), and ellipsoidal multivariate trimming (MVT) can be used. A multiple outlier detection algorithm, closest distance to center (CDC), is proposed in this paper. CDC is conceptually similar to SHV but computationally more efficient than SHV. The use of the Mahalanobis distance in the initial step of MVT is known to be ineffective for detecting outliers. To overcome this limitation, CDC is incorporated with MVT. To increase the sensitivity for outlier detection for SHV, CDC, and MVT, a new modified scaling approach is proposed.

With the representative normal data identified and a model for the process constructed , the next step is to apply the model for on-line process monitoring. Once a fault is detected on-line, the immediate step is to determine the root cause. The objective of fault identification is to determine the variables that are most relevant to diagnosing the fault, thereby focusing the plant operators and engineers on the subsystem(s) where the fault has most likely occurred.

The contribution chart is a commonly used technique for fault identification. Previous results show that contribution charts perform well for simple faults, but are less effective for identifying complex process faults (MacGregor and Kourti, 1995). This demonstrates the need to look for an alternative method for identifying process faults. In this paper, GAs are incorporated with Fisher discriminant analysis (FDA) for process fault identification

2. METHODS

2.1 Effect of Scaling

Auto scaling is commonly applied to multivariate data. For a data sequence $\{x_i\}$, the auto scaling procedure follows:

$$d_i = \frac{x_i - m_x}{s}$$

where m_x is the mean of the variable and s is the standard deviation. For data that follow a normal distribution, the probability that $|d_i| > 3$ is about 0.27%. In the commonly used "3σ edit rule", an observation x is regarded as an outlier when $|d_i| > 3$. In the presence of multiple outliers, the 3σ edit rule can perform poorly. This is demonstrated in Fig. 1a, in which observations 1-960 are normal data and observations 961 to 1440 are outliers. By definition outliers are data that are not consistent with the majority of the data. The mean and standard deviation of the normal data are 41.1 and 0.55, respectively. With multiple outliers occurring on the same side of the mean, the estimate of the mean of the entire data sequence is increased to 42.3. These outliers also inflate the standard deviation estimate more than threefold to 1.87. The 3σ edit rule fails to detect the outliers (*i.e.*, $|d_i| < 3$ for all observations in Fig. 1b).

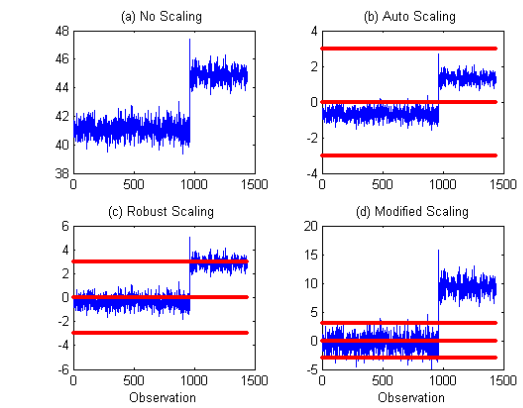

Fig. 1. Comparison of various scalings on the same variable. Observations 1-960 represent normal data and observations 961-1440 represent outliers. The solid lines represent the ±3σ thresholds.

To reduce the effect of multiple outliers, robust scaling has been suggested (Huber, 1989). In robust scaling, the mean is replaced with median and the standard deviation is replaced with median absolute deviation from the median (MAD):

$$s_{MAD} = 1.4826 \underset{i}{median}\left\{\left|x_i - x_{median}\right|\right\}$$

where x_{median} is the median of x. For the data used in Fig. 1, the median is 41.9, which is a fairly accurate location estimate for the normal data. The MAD for the data sequence is 1.17, which is a twofold overestimate. The 3σ edit rule with robust scaling, commonly referred to as the Hampel identifier (Pearson, 2001) fails to detect 60% of the outliers (see Fig. 1c).

Modfied scaling. To further increase the sensitivity in detecting outliers, a modified scaling is proposed here. For a variable with n observations, the $n/2$ observations that are nearest to the median are determined. The mean and standard deviation of these observations are used to autoscale the entire data sequence. For the data used in Fig. 1, the estimates of the mean and standard deviation are 41.3 and 0.39, respectively, which are close to the mean, 41.1, and standard deviation 0.55, found using the normal data only. With modified scaling, almost all the normal data are inside the 3σ thresholds while all the outliers are outside the 3σ thresholds (see Fig. 1d).

2.2 Robust outlier detection algorithms

Resampling by Half-Means (RHM): Given a data set of n observations and m process variables, a n by m matrix X is constructed. To start RHM, the first sample (i = 1) is obtained by randomly selecting half of the total observations. The sample i is written as a $n/2$ by m matrix $X_{sam}(i)$ and the mean $m(i)$ and standard deviation $s(i)$ vectors of the columns of $X_{sam}(i)$ are determined. The original data matrix X is autoscaled using $m(i)$ and $s(i)$, which results in a n by m autoscaled matrix X(i). The Euclidean distance is determined for each observation and a n by 1 vector of vector lengths $l(i)$ is obtained. The data are resampled for at least 2n times (Egan and Morgan, 1998). All the vector lengths are then stacked into an n by 2n matrix L. With sufficient resamplings, it is expected that the outliers will dominate in the upper (1-c) portion of L. For robust RHM, $m(i)$ and $s(i)$ are replaced with median and MAD, respectively.

Smallest Half Volume (SHV): In SHV (Egan and Morgan, 1998), the matrix X is first autoscaled and the Euclidean distance between each pair of observations i and j is determined. An n by n distance matrix D is formed and each column is sorted in ascending order. The column with the smallest sum for the first $n/2$ smallest distances is determined. These are the $n/2$ observations that are closest to each other in the multivariate space, which represent the most consistent portion of the normal data for most cases. In robust SHV and modified SHV, robust scaling and modified scaling are applied, respectively, to the matrix X first. The remaining steps are the same as the standard SHV.

Closest Distance to Center: CDC identifies the most consistent observations by calculating the distance of each observation from the center (i.e., mean for autoscaling and median for robust scaling) (Chiang *et al.*, 2003). In CDC, the matrix X is first autoscaled and the distance is determined for each observation. To equally weight the contribution for each variable to the distance, Euclidean distance (2-norm distance) can be used for each observation. This implementation is referred to as CDC_2. To emphasize

the most significant contribution of the variable to the distance, the maximum norm distance can be used for each observation. This implementation is referred to as CDC_m. The n/2 observations with the smallest distances represent the portion of the data that are closest to the center. Assuming that outliers are extreme observations that are far away from the majority of the data, these n/2 observations represent a portion of the normal data. Recall that the mean is not an accurate representation of the center of the data. A better implementation of CDC_2 and CDC_m is to use robust scaling or modified scaling prior to the distance determination steps.

Ellipsoidal Multivariate Trimming (MVT): MVT is an iterative procedure for the determination of a robust covariance matrix (Walczak and. Massart, 1995). In the first step of MVT, the Mahalanobis distance is determined for observation **x**

$$d_{mah} = (\mathbf{x} - \mathbf{x}^*)^T S^{*-1} (\mathbf{x} - \mathbf{x}^*)$$

where **x*** is the mean and S* is the covariance, calculated using all *n* observations. The *n*/2 observations with the smallest Mahalanobis distances are determined. Such observations are used to determine the new mean **x*** and new covariance S*. The Mahalanobis distance is recalculated using the new mean **x***, the new covariance S*, and the old **x**. The iterative procedure continues until *x** and S* stabilize.

With the presence of multiple outliers in the original data set, the covariance structure is disrupted. The use of Mahalanbis distance in the initial step of MVT can result in masking and swamping. As such, it is possible that further iterations in MVT do not improve the outlier detection proficiency. To overcome this weakness, robust outlier detection techniques such as RHM, SHV, CDC_2, or CDC_m can be used to determine the most consistent *n*/2 observations. These observations are then used to calculate **x*** and S*, upon which the initial Mahalanobis distance is calculated. In this paper CDC_m is used in conjunction with MVT. This implementation is referred to as CDC_m/MVT. Robust scaling and modified scaling are also applied in MVT and CDC_m/MVT.

2.3 Fault detection and fault identification

Principal Component Analysis: PCA is a well-known multivariate technique and detailed descriptions on the subject are available elsewhere (Chiang *et al.*, 2001; Beebe *et al.*, 1998). Only a brief review is given here. The PCA model is calculated using the singular value decomposition (SVD) on the autoscaled data matrix X

$$\frac{1}{\sqrt{n-1}} X = U\Sigma V^T$$

The loading vectors V corresponding to the *a* largest singular values are typically retained. These vectors are then stacked into an *m* by *a* loading matrix P. For on-line fault detection using the score space, the T^2 statistic can be calculated directly from the PCA representation (Jackson, 1959).

$$T^2 = \mathrm{x}^T P \Sigma_a^{-2} P^T \mathrm{x} = \mathrm{t}^T \Sigma_a^{-2} \mathrm{t}$$

where **t** is an *n* by 1 score vector, and S_a contains the first *a* rows and columns of Σ.

The portion of the observation space corresponding to the *m-a* smallest singular values can be monitored using the Q statistic (Jackson and Mudhlkar, 1979)

$$Q = \mathbf{x}^T (I - PP^T)\mathbf{x}$$

Contribution Chart: After a fault is detected (T^2 or Q statistics are larger than the threshold), the next step is to determine the root cause of the fault. While decentralized PCA techniques can often effectively isolate the location of the fault for large-scale systems (Georgakis *et al.*, 1996; Wachs and Lewin, 1999), the aim of the contribution chart is to determine the abnormal variables by calculating the contribution of each variable to the T^2 and Q statistics (Miller and Swanson, 1998). Detailed procedure to implement contribution charts is available elsewhere (MacMregor and Kourti, 1995; Chiang *et al.*, 2001).

Fisher Discriminant Analysis: FDA is a linear dimensionality reduction technique, optimal in terms of maximizing the separation between several classes (Duda and Hart, 1973). The FDA vectors are equal to the eigenvectors, $\mathbf{w_i}$, of the generalized eigenvalue problem

$$S_b \mathbf{w_k} = l_j S_w \mathbf{w_k}$$

where S_b is the between-class scatter matrix, S_w is the within-class scatter matrix, and the eigenvalues $ë_k$ indicate the degree of overall separability among the classes by projecting the data onto $\mathbf{w_k}$.

For classification, the discriminant function is calculated for class $j = 1$ to *c*. An observation **x** is assigned to class *j* that maximizes the discriminant function. Akaike's information criterion has been developed for automatically selecting the rank for FDA using the fitness function (Chiang, *et al.*, 2001)

$$f_{FDA} = s(a) - \frac{a}{n_{avg}}$$

where *s(a)* is the cross validation classification success rate at FDA rank *a* and n_{avg} is the average number of observations per class. The fitness function is calculated for $a = 1$ to $\min(m,n)$. The maximum fitness value, $f_{FDA,opt}$, represents the classification results at the optimal rank.

Genetic Algorithms: Once a fault is detected on line using PCA, GA/FDA can be used to determine the variables responsible for the root cause. A detailed review of GAs is available elsewhere (Leardi, 2001; Leardi *et al.*, 1992), only a brief review is given here. Two classes of data are used in FDA. Class 1 contains the training data representing the normal operating conditions. Class 2 contains data from a

time in which a fault is known or suspected to have occurred. GA/FDA begins with a first run by randomly creating n_p chromosomes. Only a subset of the original variables is selected in each chromosome. The performance of each chromosome is evaluated using a leave-1/5-out cross validation scheme with FDA. The fitness function $f_{FDA,opt}$ is then calculated for all chromosomes. Cross-over and mutations are performed over the evolutions in order to improve the chromosomes (*i.e.*, increase the fitness function $f_{FDA,opt}$). At the end of n_e evolutions, the chromosome with the highest $f_{FDA,opt}$ is saved.

The procedure is repeated for a second run. The final chromosome with the highest $f_{FDA,opt}$ at the end of n_e evolutions is saved. At the end of the n_r runs, n_r chromosomes are retained. A bar chart of the frequency of selection of each variable is then constructed. The plot represents the importance of each variable for distinguishing between the two classes. If the fitness function is high (*i.e.*, high success rate in cross-validated classification), these variables are often correlated with the root cause of the process fault. The variables are sorted according to the frequency of selection. The number of variables required to explain the root cause can be determined by maximizing the fitness function

$$f_{GA/FDA} = f_{FDA,opt}(m_{sub}) - \frac{m_{sub}}{n_{avg}}$$

where m_{sub} is the number of retained variables, corresponding to the first m_{sub} highest selected variables.

3. APPLICATIONS

Fig. 2 is a process flowsheet for the Tennessee Eastman Process (TEP). The TEP is based on an industrial process where the components, kinetics, and operating conditions were disguised for proprietary reasons (Downs and Vogel, 1993). The gaseous reactants A, C, D, and E and the inert B are fed to the reactor where the liquid products G and H are formed. The plant-wide control structure recommended in Lyman and Georgakis (1995) was implemented to generate the closed loop simulated process data for each fault.

TEP can simulate 21 process faults; Fault 6 is studied in detail in this paper. For Fault 6, there is a feed loss of reactant A in Stream 1 at t = 24 hr (see variable 1 in Fig. 3), which causes the control loop on Stream 1 to fully open the A feed valve (see variable 44 in Fig. 3). Because there is no reactant A in the feed, the reaction will eventually stop. This causes the gaseous reactants D and E to build up in the reactor, and hence the reactor pressure increases (see variable 7 in Fig. 3). The reactor pressure continues to increase until it reaches the safety limit of 2950 kPa, at this point the valve for Control Loop 6 is fully open. Clearly, it is very important to detect this fault promptly before the fault upsets the whole process. The proficiencies of contribution charts and GA/FDA are evaluated in terms of correctly identifying the root cause for Fault 6.

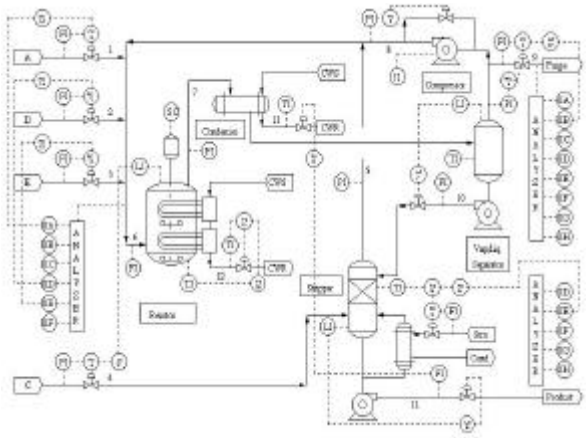

Fig. 2. A process flowsheet for the TEP

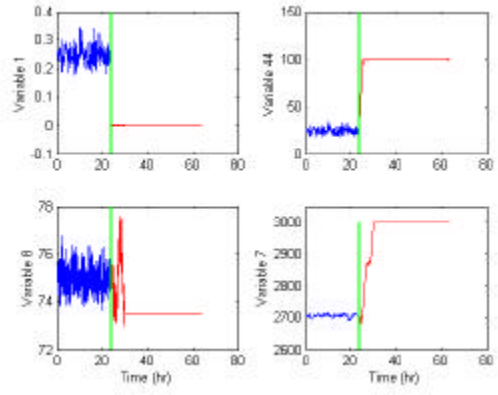

Fig. 3. The time series plots for the reactant A feed flow (variable 1), the reactant A feed valve (variable 44), the reactor level (variable 8), and the reactor pressure (variable 7). Fault 6 occurs at t = 24 hr.

To evaluate the outlier detection algorithms, 960 normal data and 480 Fault 6 data were generated. The outlier detection algorithms were used to identify the most consistent 720 observations (half of the total samples). The performance was evaluated in terms of the number of correctly identified normal data in those 720 observations.

4. RESULTS AND DISCUSSION

4.1. Outlier detection

For the original RHM algorithm, it is suggested that the upper 5% (cutoff point = c = 0.95) of the vector lengths should be checked for outliers. It is important to note that the cutoff point is correlated with the number of outliers in the data set. For a data set with large numbers of outliers, a lower cutoff point is desired. For c = 0.95, only the most extreme outliers

were identified. As c decreased to 0.75, RHM detects more outliers. As c decreases to 0.5, the swamping effect is observed. A tuning procedure is required in order to determine the optimal cutoff point for a given data set.

One way to determine the optimal cutoff point is to plot the histogram of the vector lengths from all resampling experiments (see Fig. 4). A cutoff point can be chosen as the point in which two distinct distributions are seen. For Fault 6 data, a cutoff point corresponding to a vector length of 8 would appear optimal and 93.3% were correctly identified as normal data.

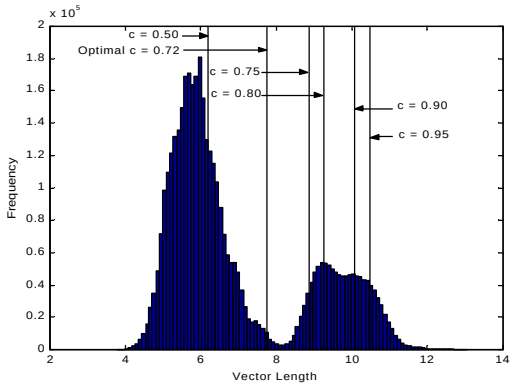

Fig. 4. The histogram of the vector lengths for the normal and Fault 6 data using RHM.

All versions of SHV correctly identify the normal data for more than 99% of the observations. The motivation to use CDC_2 or CDC_m is that they are conceptually similar to SHV, and the computation time is far less. For a data set with n observations, it is required to compute $n(n\text{-}1)/2$ Euclidean distances for SHV, versus n Euclidean distances for CDC. In other words, CDC runs $(n\text{-}1)/2$ times faster than SHV. The saving in computation time is significant when n is large.

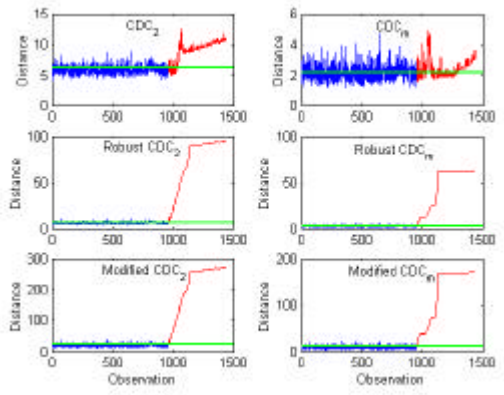

Fig. 5. The distances using CDC. Observations 1-960 represent normal data and observations 961-1440 represent Fault 6 data. Solid line represents median of the distance.

Fig. 5 displays the Euclidean distances and maximum-norm distances for CDC_2 and CDC_m, respectively. Robust CDC_2, robust CDC_m, modified CDC_2, and modified CDC_m all resulted in 100% success rate in identifying normal data. This suggests that all outliers are far away from the median and that it is a good measure to identify normal data based on the nearest distances to the median for Fault 6 data. While CDC_2 and CDC_m are able to identify the majority of the normal data, they are far less sensitive than the robust and modified version of CDC. This indicates that the mean of all of the observations is different than the mean of the normal data and the outliers have disrupted the estimation of the true mean of the normal data.

The initial step of MVT requires computation of the Mahalanobis distance, which is found to be an ineffective step for identifying outliers. This is shown in Fig. 6, in which the Mahalanobis distances are plotted for MVT, robust MVT, and modified MVT after the first and tenth iterations. For the first iteration of MVT, the half of the total observations with the smallest Mahalanobis distances were contaminated with outliers, further iterations did not improve the proficiency of MVT. For robust MVT and modified MVT, the half of the total observations with the smallest Mahalanobis distances contains mainly normal data. In this situation, further iterations do improve the proficiency of MVT.

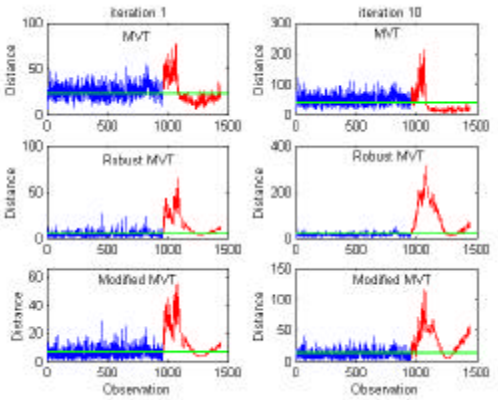

Fig. 6. The distances using MVT for iterations 1 and 10. Observations 1-960 represent normal data and observations 961-1440 represent Fault 6 data. Solid line represents median of the distance.

Robust CDC_m and modified CDC_m result in an accurate estimation of the mean and covariance of the normal data. Further iterations improve the proficiency of MVT slightly.

4.2 Fault detection and identification

Fault 6 occurs at t =24 hr. For time period 24-29 hr, GA/FDA selects the reactant A feed flow (variable 1) 99 times (see Fig. 7), indicating that this variable is strongly related to the root cause of Fault 6. The optimal fitness function $f_{GA/FDA,opt}$ is 0.993 (corresponds to 100% correct in cross validated classification result) when a single variable, reactant

A feed flow, is selected. At the same time period, the T^2 statistic contribution chart indicates that the reactant A feed valve (variable 44) contributes the most to Fault 6 and the Q statistic contribution chart indicate that the reactant A feed flow (variable 1) contributes the most to Fault 6 (see Fig. 7). Using GA/FDA provides more direct indication for the root cause.

For time period 29-34 hr, Fault 6 propagates to more than half of the total variables in the process. It will be more difficult to identify the root cause as the number of affected variables increases. As shown in Fig. 7, the reactant A feed flow (variable 1) is still selected the most by GA/FDA, although the frequency of selection decreases to 18. The contribution charts indicate that the stripper pressure (variable 16), the reactor cooling water valve (variable 51), the stripper steam valve (variable 19), and the separator pressure (variable 13) contribute the most to Fault 6 at this time period (see Fig. 7). Time series plots for these four variables show that significant step changes are found. While contribution charts detect changes in the variables for Fault 6, this does not directly lead to diagnosing the root cause (Loss of component A in feed stream 1)

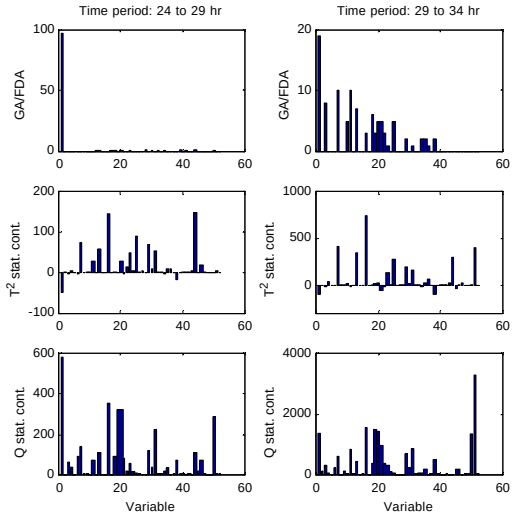

Fig. 7. The variable selection using GA/FDA, the T^2 statistic contribution chart, and the Q statistic contribution chart for the period between 24-29 hr (left hand side of the plot) and between 29-34 hr (right hand side of the plot).

5. CONCLUSIONS

To extract normal data from a historical database, robust outlier detection algorithms such as RHM, SHV, MVT, and CDC can be used. Using CDC as an initial estimate in MVT results in the best overall results using the Tennessee Eastman process data. Modified scaling is more sensitive in detecting outliers.

GA/FDA correctly identifies the variables that are responsible for the root causes for the TEP data. For cases where the process fault propagates downstream and affects more variables, GA/FDA has a better persistence in identifying the root causes as compared to contribution chart

REFERENCES

Beebe, K. R., R. J. Pell and M. B. Seasholtz (1998). *Chemometrics: A Practical Guide*, John Wiley & Sons.

Chiang, L. H., E. L. Russell and R. D. Braatz (2001). *Fault Detection and Diagnosis in Industrial Systems*, Springer-Verlag.

Chiang, L. H., R. J. Pell and M. B. Seasholtz (2003). Exploring process data with the use of robust outlier detection Algorithms. *J. of Process Control*, (in press)

Downs, J. J and E. F. Vogel (1993). A plant-wide industrial process control problem. *Comp. & Chem. Engr.*, **17,** 245-255

Duda, R. O. and P. E. Hart (1973). *Pattern Classification and Scene Analysis*, John Wiley & Sons

Egan, W. J. and S. L. Morgan (1998). Outier detection in multivariate analystical chemical data. *Anal. Chem.*, **70,** 2372-2379.

Georgakis, C., B. Steadman and V. Liotta (1996). Decentralized PCA Charts for performance assessment of plant-wide control structures. In *Proc. of the 13th IFAC World Congress***,** 97-101, IEEE Press, New Jersey

Huber, P. (1989). *Robust Statistics*, John Wiley & Sons

Jackson, J. E. (1959). Quality control methods for several related variables. *Technometrics*, **1,** 359-377.

Jackson, J. E. and G. S. Mudhlkar (1979). Control procedure for residuals associated with principal component analysis. *Technometrics*, 2**1,** 341-349

Leardi, R. (2001). Genetic algorithms in chemometricsand chmistry: a review. *J. of Chemometrics*, **15,** 559-569.

Leardi, R., R. Boggia and M. Terrile (1992). Genetic algorithms as a strategy for feature selection. *J. of Chemometrics*, **6,** 267-281.

Lyman, P. R. and C. Georgakis (1995). Plant-wide control of the Tennessee Eastman problem. *Comp. & Chem. Engr.*, **19,** 321-331.

MacGregor, J. F and T. Kourti (1995). Statistical process control of multivariate process. *Control Engr. Practice*, **3,** 403-414.

Miller, P. and R. E. Swanson (1998). Contribution plots: a missing link in multivariate quality control. *Appl. Math. and Comp. Sci..*, **8,** 775-792.

Pearson, P. K. (2001). Exploring process data. *J. of Process Control*, **11,** 179-194.

Wachs, A and D. R. Lewin. (1999). Improved PCA methods for process disturbance and failure identification. *AIChE J*, **45,** 1688-1700.

Walczak, B. and D. L. Massart (1995). Robust principal components regression as a detection tool for outliers. *Chemom. Intell. Lab. Syst.*, **27,** 41-52